Chapter 3

K-edge applications

In this chapter, the results of elemental imaging on some mock-ups of pigments based on cadmium, copper and cobalt, using the technique of balanced filters will be presented. The filter used are shown in the Figure 3.1 and their thickness has been reported in Table 2.2 and 2.3 in Chapter 2. Thanks to a filter-holder, already present at the exit window of the X-ray tube, the K-edge technique using balanced filters can be applied with the two radiographic scanner described in the previous chapter.

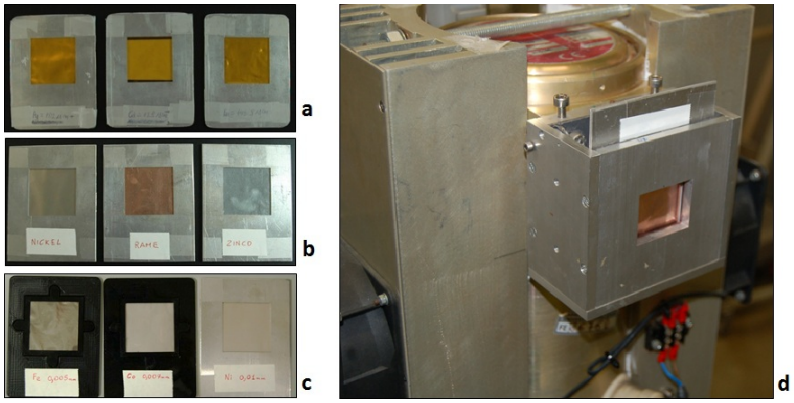

Figure 3.1: a) Filters of Ag, Cd and In. b)Filters of Ni, Cu and Zn. c) Filters of Fe, Co and Ni. d) Detail of the filter-holder of the X-ray tube

The test objects are little canvases (10 x 10 cm) painted with selected pigments. They are of two types. First, in which the same pigment has been applied from 1 to 5 times in order to obtain a gradation in the content of the pigment to test the system sensitivity. Due to manual application, the scale of the target element is not necessarly linear, even if the number of brushstrokes is linearly increasing. The other, in which two different pigments are overlapping in the central area to identify different layers (Figure 3.2). For cadmium, the mock-ups have been realized by the Cultural Heritage Restoration and Conservation Center "La Venaria Reale" in Turin, and some have been already analysed with the first goniometric system [28] and balanced filters [24]. The samples for copper and cobalt have

been realized by the restorer Emanuela Ruggio[1], on a unique bigger canvas, maintaining the areas of 10 x 10 cm for each type.

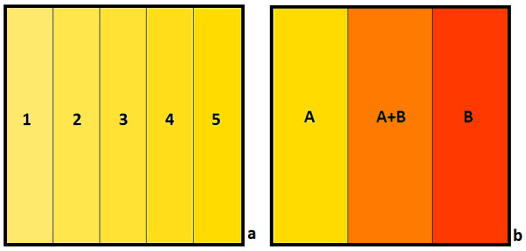

Figure 3.2: Schemes of the two types of mock-ups: a) the gradation of pigment, b) the overlapping of two pigments

All the greylevels that will be shown in this chapter are the result of the digital elaboration of the images, following the KES and Lehmann Algorithms. The pixel content of the images has been converted to a real value 32 bit long, so the results of the algorithms are coded in numbers spanning from - 2147483648 up to + 2147483648. We refers to these numbers as greylevel*, just to remind that they are the results of elaboration of the greylevel of the original images. The greylevel* reported in the plots are calculate(by ImageJ[2] software) as mean values on areas identified on the images, and the error bars correspond to the standard deviation computed on the same area. In Figure 3.3, an example of the box considered for the KES radiography of the cadmium yellow canvas is reported.

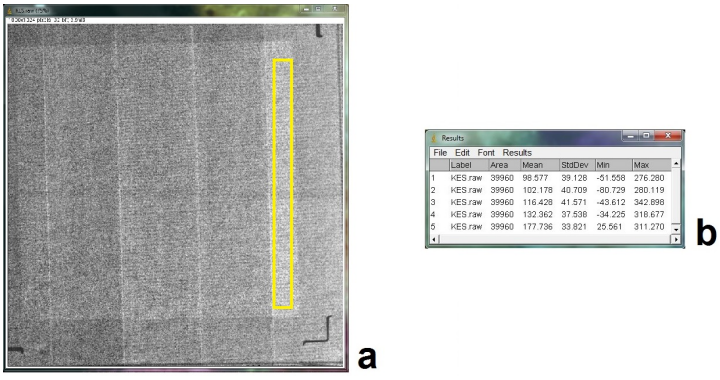

Figure 3.3: KES radiography of cadmium yellow gradation canvas: a) KES image, in yellow the area considered for the 5 brushstrokes; b) table of the values measured for the 5 areas

All the areas of the canvases have been also analysed by XRF technique. The instrument used is the ARTAX 200[3] with Mo X-ray tube.

[1]E. Ruggio, Restauro "la conservazione dell'arte", (Vittorio Veneto, Italy)
[2]https://imagej.nih.gov/ij/
[3]https://www.bruker.com Bruker GmbH (Germany)

The XRF results reported in this chapter are the mean of the counts per second (cps) acquired on 2-3 spots per area, because the brushstrokes are not homogeneous, and the error lines represent the variability of these data in the same area. It is always bigger of two orders of magnitude than the error of the single measurement.

3.1 Cadmium

For cadmium the two selected pigments to be analysed are cadmium yellow[4] (cadmium zinc sulphide, (Cd,Zn)S) and cadmium red[5] (cadmium sulfoselenide, Cd_2SSe), mixed with linseed oil as medium. The Figure 3.4 shows the two canvas with the scale of pigment ("a" type).

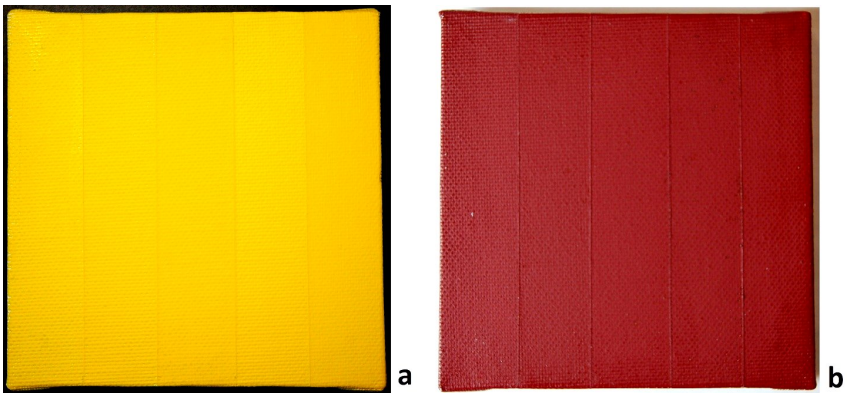

Figure 3.4: Cd test objects "a" type: a) Cd Yellow, b) Cd Red

The little canvases with the overlapping of two pigments are three:

- Naples yellow[6] (lead antimonate, $Pb_2Sb_2O_7$) and cadmium yellow,
- cadmium yellow and realgar[7] (arsenic sulfide, As_4S_4),
- Naples yellow and cadmium red,

as reported in Figure 3.5.

[4] n° 21020, Kremer Pigmente GmbH (Aichstetten, Germany)
[5] n° 21140, Kremer
[6] n° 43125, Kremer
[7] n°10800, Kremer

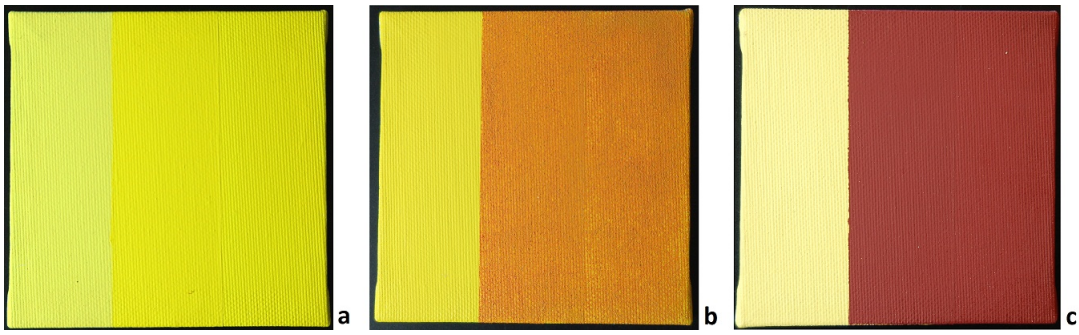

Figure 3.5: Cd test objects "b" type: a) Naples yellow and cadmium yellow, b) cadmium yellow and realgar, c) Naples yellow and cadmium red

3.1.1 KES technique

Performing the K-Edge Subtraction (KES) technique, for all the Cd canvases, three radiographies have been acquired with the filters of silver, cadmium and indium. The elaboration has been made subtracting the Ag image from the Cd one, in order to obtain the Low Energy image, and the Cd image from the In one, obtaining the High Energy image.

Cadmium yellow

In the Figure 3.6, the results of the KES technique for **cadmium yellow** are shown. The two images a) and b) are the Low and High energy images respectively. Subtracting the second to the first one, the KES image is obtained (c). Higher greylevels* correspond to a major content in cadmium, in area with the same characteristics.

The graph d) in Figure 3.6 highlights that with the XRF technique, increasing the number of brushstrokes, then the Cd quantity increases, too. The greylevels* in the area 1 and 2 are the same. This may be due to the fact that this technique seems to be less sensitive than XRF if the thickness is near to the minimum detectable quantity.
However, also the greylevels* seem to follow the content of cadmium in this case.

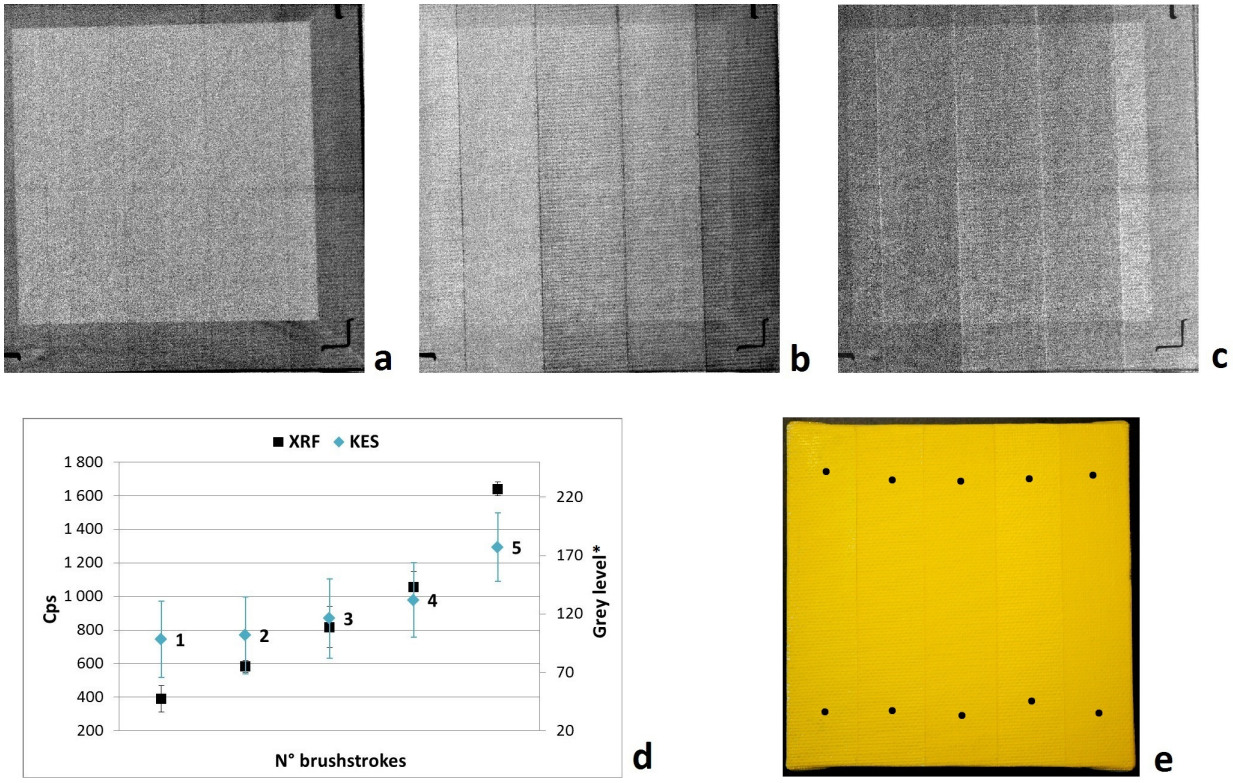

Figure 3.6: KES radiography of cadmium yellow: a) Low Energy image, b) High Energy image, c) KES image, d) counts per second on Cd peak from the XRF analysis (50 kV, 700 μA, 60 s) and mean greylevel for each area (N° of brushstrokes), e) color photo of the test object with the XRF spots (Black). RX acquired at 35 kV, 60 mA, 1 mm Al, 750 ms, W anode.

Cadmium red

The Figure 3.7 shows similar results for the **cadmium red** pigment. In this case the settings employed are the same of the cadmium yellow, but gave a worse KES image (c). It is evident that in this image there is low contrast between the 5 areas. It is due to a lower number of photons impinging on the detector or to small differences in the Cd quantity for each zone. This is confirmed also by the measured greylevel* means in the graph (d): considering the big error lines a really separation between the five areas cannot be done.

However, the greylevels* follow the same trend of the XRF analysis, which shows an higher content of cadmium for the section 2, similar to the 4^{th}.

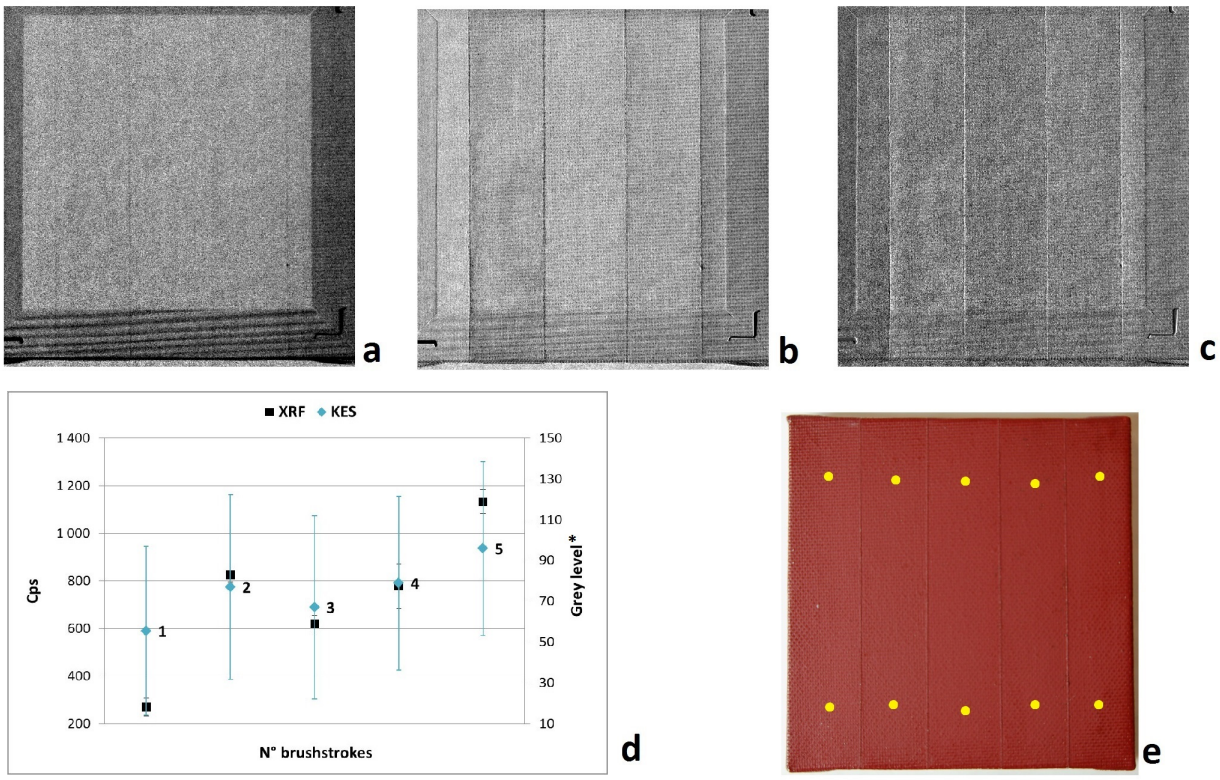

Figure 3.7: KES radiography of cadmium red: a) Low Energy image, b) High Energy image, c) KES image, d) counts per second on Cd peak from the XRF analysis (50 kV, 700 μA, 60 s) and mean greylevel* for each area (N° of brushstrokes), e) color photo of the test object with the XRF spots (Yellow). RX acquired at 35 kV, 60 mA, 1 mm Al, 750 ms, W anode.

To enhance the contrast of the KES image, new measurements have been done increasing the time of acquisition from 750 ms to 1 s, in order to have a higher number of photons transmitted by the sample. The results are reported in Figure 3.8. The KES image (c) is now more contrasted and the relative greylevels* have a wider spread (d).

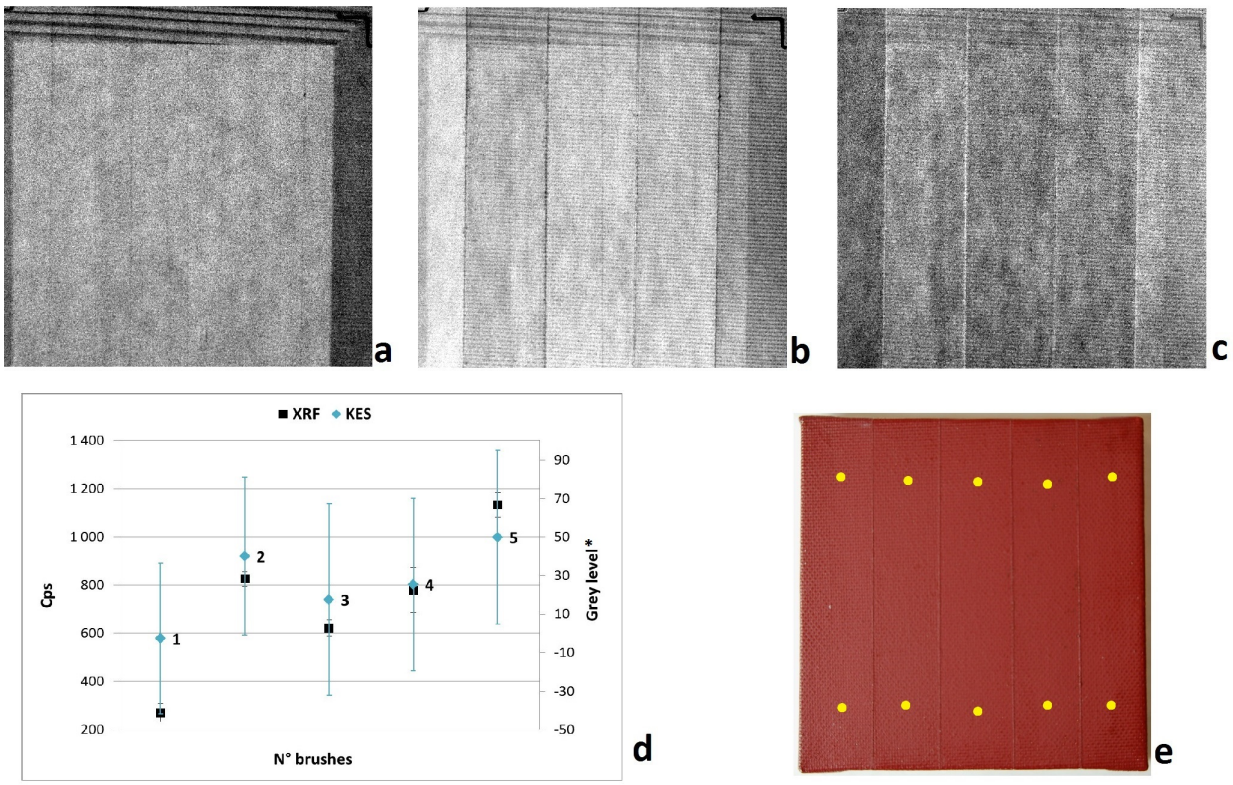

Figure 3.8: KES radiography of cadmium red: a) Low Energy image, b) High Energy image, c) KES image, d) counts per second on Cd peak from the XRF analysis (50 kV, 700 μA, 60 s) and mean greylevel* for each area (N° of brushstrokes), e) color photo of the test object with the XRF spots (Yellow). RX acquired at 35 kV, 60 mA, 2 mm Al, 1 s, W anode.

Considering the greylevels* of these two mock-ups (Figure 3.9), their fitting curves indicate that the amount of cadmium is near the limit of detectable quantity. Indeed, the three curves are almost flat and near to the minimum of the function. Furthermore, looking at the graph b) regarding the Cd red mock-ups, the time increase (KES2) helped the greylevels* distancing slightly.

Passing to the three mock-ups with two pigments overlapping, during the elaboration, the radiographies acquired with the Cd filter have been multiplied for 1.2 as corrective factor.

As can be seen in Figure 3.10, the differences between the spectra acquired with the three filters simulate the virtual beam which could generate the Low (Cd-Ag) and the High (In-Cd) Energy images. The effects of the corrective factor are to raise the Low energy (Cd-Ag) peak and to flatten the area around the fluorescence lines of Mo (17.48 and 19.61 keV). These lines may disturb the final results, because the three radiographies acquired

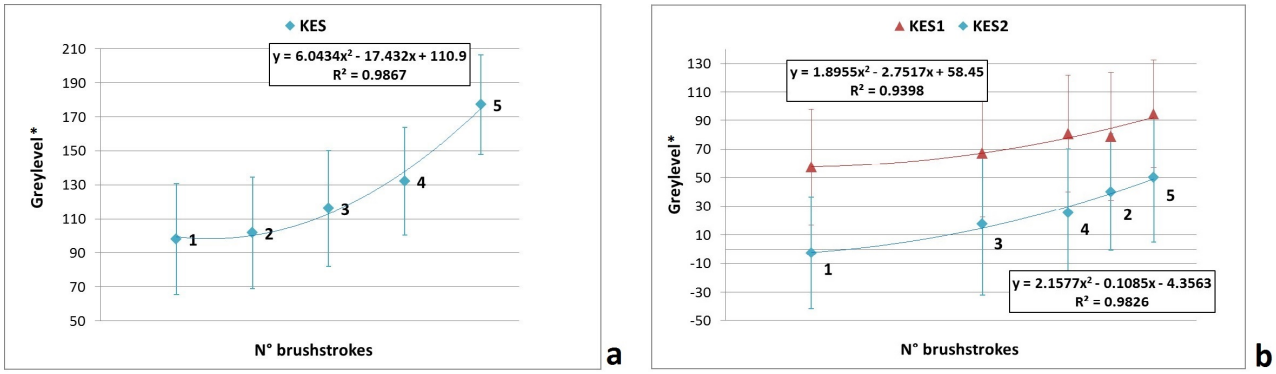

Figure 3.9: Fit of the greylevel* measured for the cadmium yellow canvas (a) and the cadmium red canvas (b). In this graph the two KES measurements are reported, and the area number 2 has been moved near the 4

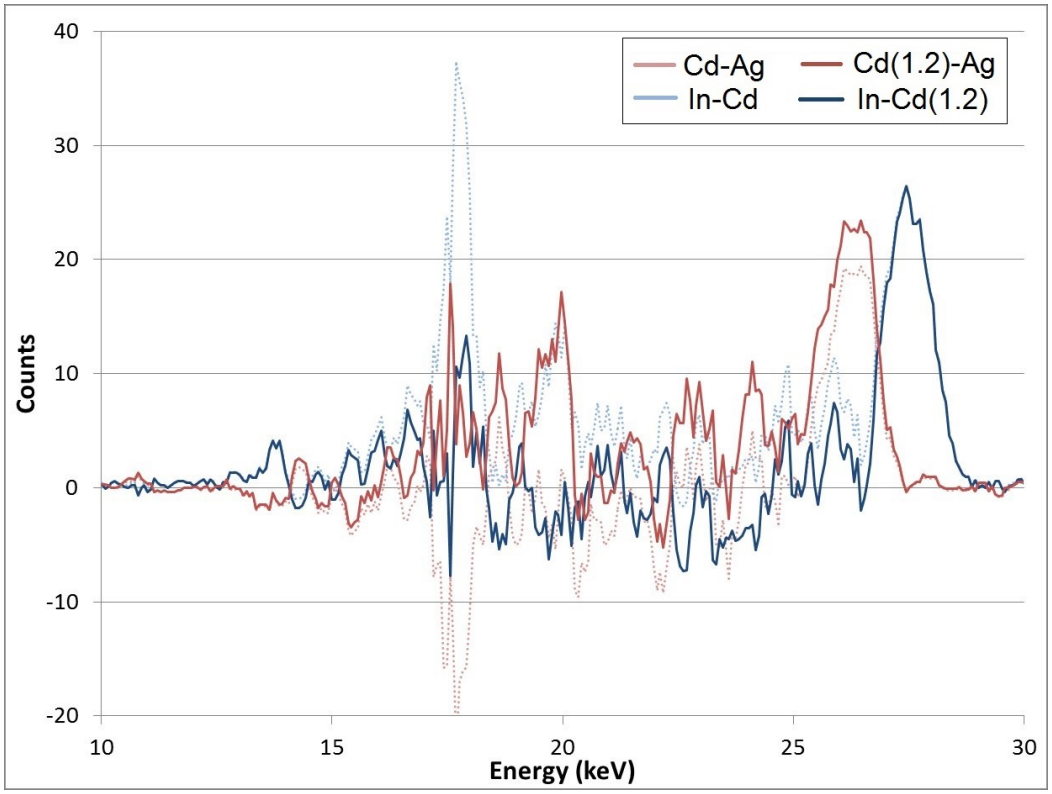

Figure 3.10: Differences between the spectra acquired with the Ag, Cd and In filters. For the darker colours the Cd spectrum has been multiplied for 1.2

may content their contribution.

Naples and cadmium yellow

Starting with the **Naples and cadmium yellow** sample, looking the photo (e) in Figure 3.11, in the left side of the canvas there is Naples yellow, while on the right it is the cadmium yellow. In the central portion, the two pigments are superposed.
However, the KES image is lighter only in the right side and not in the central area, even if cadmium is present. This disagreement is evident also in the graph (d), where the cps are similar for the central and right areas of the canvas (2 and 3, respectively), while the greylevels* give the same result for the left and central areas (1 and 2).

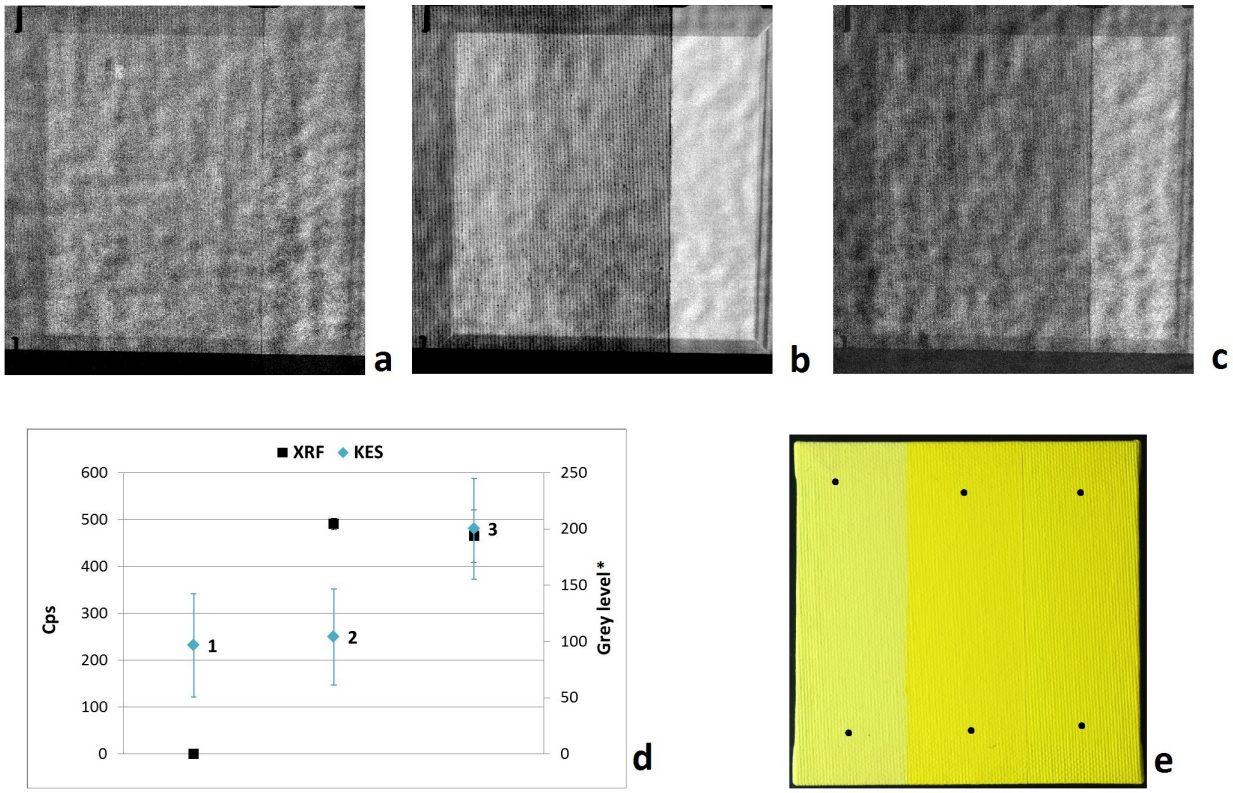

Figure 3.11: KES radiography of Naples and cadmium yellow: a) Low Energy image, b) High Energy image, c) KES image, d) counts per second on Cd peak from the XRF analysis (50 kV, 700 μA, 60 s) and mean greylevel* for each area, e) color photo of the test object with the XRF spots (black): the Cd Yellow is on the right side. RX acquired at 35 kV, 60 mA, 1.55 mm Al, 1s, Mo anode.

Remembering that Naples yellow is $Pb_2Sb_2O_7$, the presence of a such heavy element (lead), which is really radiopaque, works like a mask for cadmium, then, hiding it.

Naples yellow and cadmium red

The same behaviour has been revealed for the **Naples yellow and cadmium red** mock-up. As in the previous case, cadmium red is present on the right side, while Naples yellow on the left, and in the central part they are superposed (see e) in Figure 3.12). Again, the KES technique seems to work properly where there is only cadmium (lighter area in c), and seems to fail where the other pigment is present.

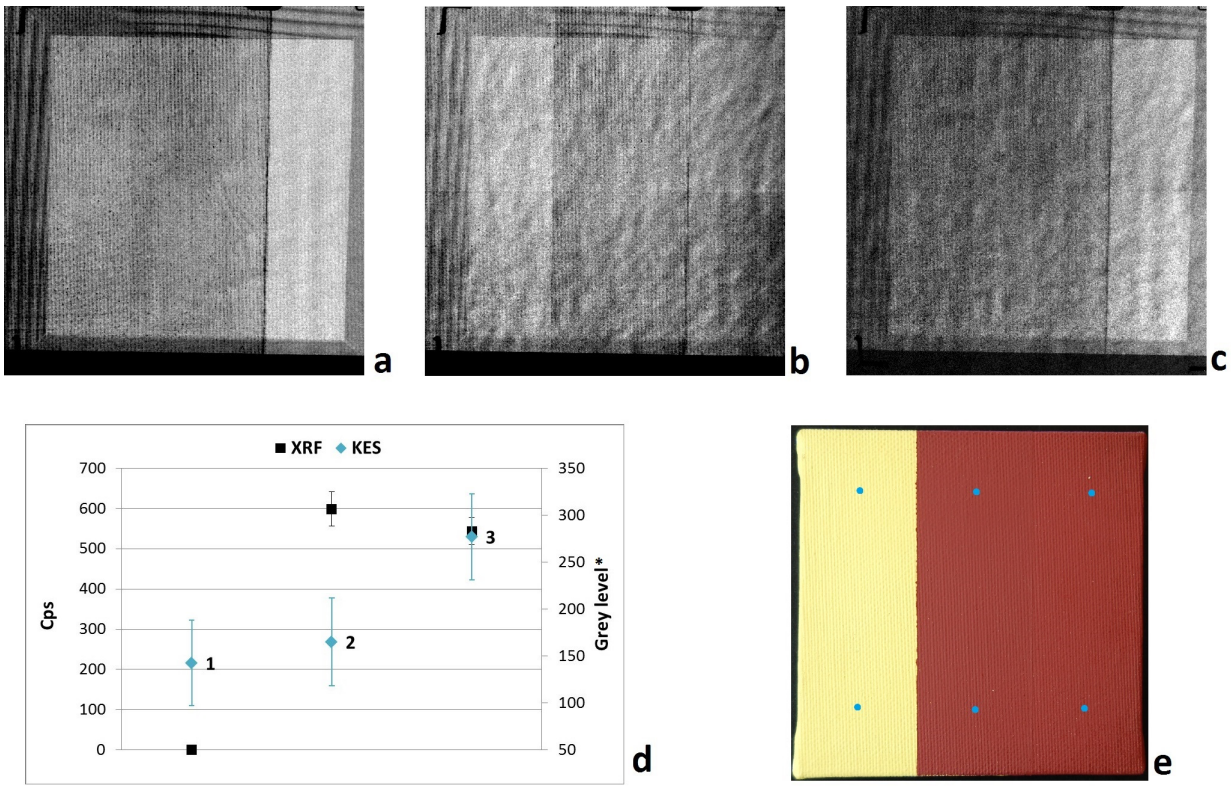

Figure 3.12: KES radiography of Naples yellow and cadmium red: a) Low Energy image, b) High Energy image, c) KES image, d)counts per second on Cd peak from the XRF analysis (50 kV, 700 μA, 60 s) and mean greylevel* for each area, e) color photo of the test object with the XRF spots (blue): the Cd Red is on the right side. RX acquired at 35 kV, 60 mA, 1.55 mm Al, 1s, Mo anode.

Furthermore, the counts in the graph (d) show an higher content of Cd in the central area, which does not correspond to the greylevels* measured in that area. So, the hypothesis that lead hides cadmium seems to be true, for the conditions in which the radiographies have been acquired.

Cadmium yellow and realgar

The third sample is the **cadmium yellow and realgar** canvas. In this case, cadmium yellow is present in the left area, while on the right there is realgar, and in the centre they

are overlapping (e in Figure 3.13). As in the previous samples, the KES image highlights the presence of cadmium where there is only the cadmium yellow (left side of c). Even if realgar is As_4S_4, and As is an element lighter than Cd, it seems to hide the cadmium itself.

Looking at the graph (d), the cps revealed in the central area (2) are less than the first one, because in this case the pigment of Cd is under the realgar, while for the other two canvases it is the upper one. So, having less counts of Cd when it is covered by other pigments, does not mean that the quantities are less.
However, the greylevels* between the areas 2 and 3, in which cadmium is absent, are the same.

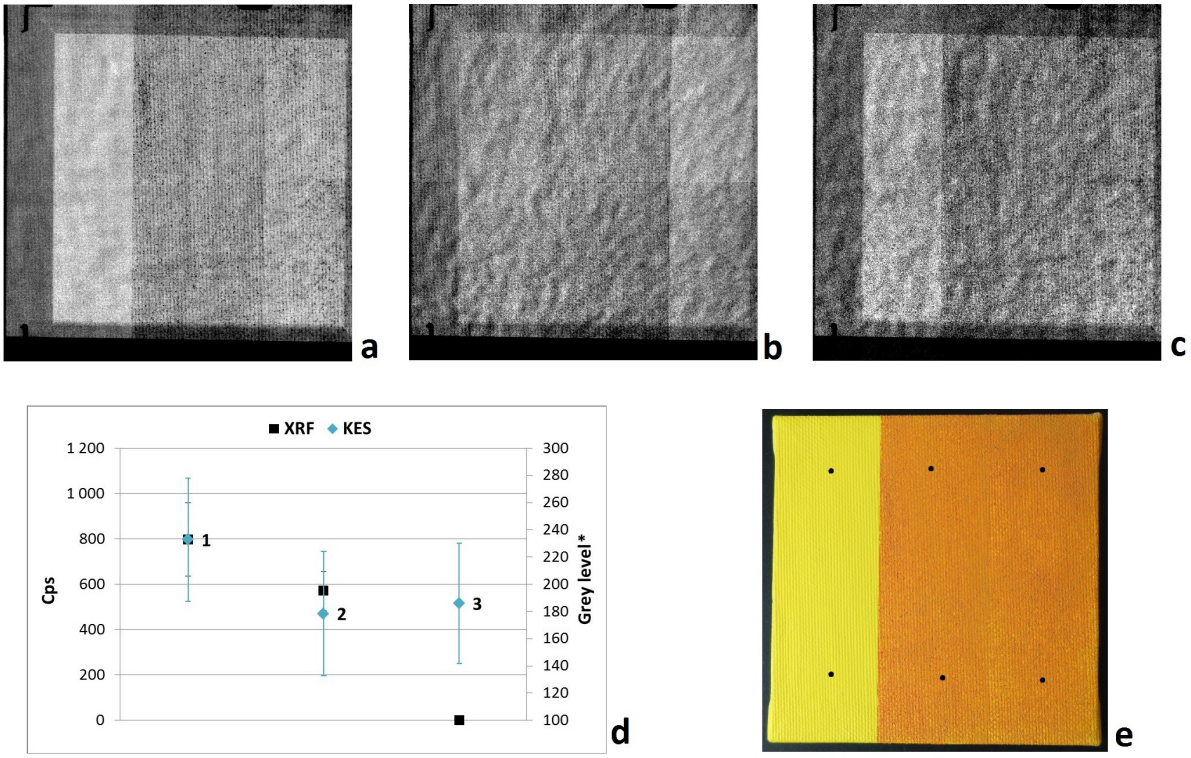

Figure 3.13: KES radiography of cadmium yellow and realgar: a) Low Energy image, b) High Energy image, c) KES image, d) counts per second on Cd peak from the XRF analysis (50 kV, 700 μA, 60 s) and mean greylevel* for each area, e) color photo of the test object with the XRF spots (black): the Cd Yellow is on the left side. RX acquired at 35 kV, 60 mA, 1.55 mm Al, 1s, Mo anode.

To conclude, working with the Mo X-ray tube in these conditions, the KES resulting image of Cadmium strongly depends by the presence of other materials and their thickness, which acts as a mask.

3.1.2 Lehmann Algorithm

The Lehmann Algorithm (Chapter 1, section 1.2) gives an image in which the greylevels* are the density ρx (g/cm^2) of the target element. It has been applied to the same images acquired with the Ag, Cd and In filters used for the KES elaboration. Considering virtual beams, under and over the K-edge of Cd, with mean energy between the K-edge of the filters, the relative absorption coefficients (μ/ρ) for cadmium (extracted by the graph in Figure 3.14) are listed in the Table 3.1.

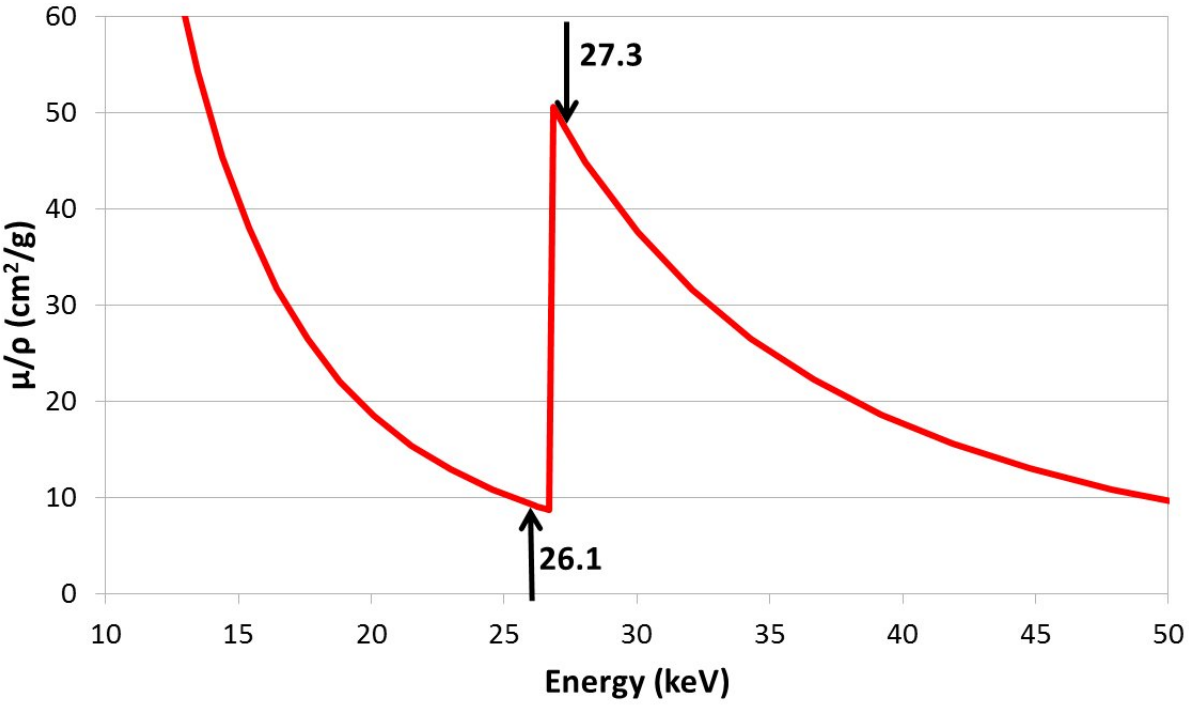

Figure 3.14: Cadmium mass absorption coefficient vs. Energy [15]

Table 3.1: Average energy and corresponding μ/ρ of cadmium

Beam	**Energy (keV)**	μ/ρ **(cm^2/g)**
Cd-Ag	26.1	~ 9
In-Cd	27.3	~ 48

The algorithm needs also the μ/ρ of an equivalent material that simulates all the others elements present in the sample. An equivalent material has been individuate as polymethylmethacrilate (PMMA) instead of the canvas [24]. Its absorption coefficients are 0.36 cm^2/g for the low energy and 0.34 cm^2/g for the high energy.

Cadmium yellow

Starting with the scale of **cadmium yellow** (from 1 at the left to 5 brushstrokes at the right), in Figure 3.15 the Lehmann image is reported (b). In this image the presence of the wood frame is less evident than in the KES image (Figure 3.6). In the graph (d), the superficial density for each area is shown. They follow the same trend of the cps and greylevel* of the graph in Figure 3.6.

However, with this analysis, the areas 1 and 2 have values under zero, which means that the content of Cadmium is near the limit of sensitivity of the technique.

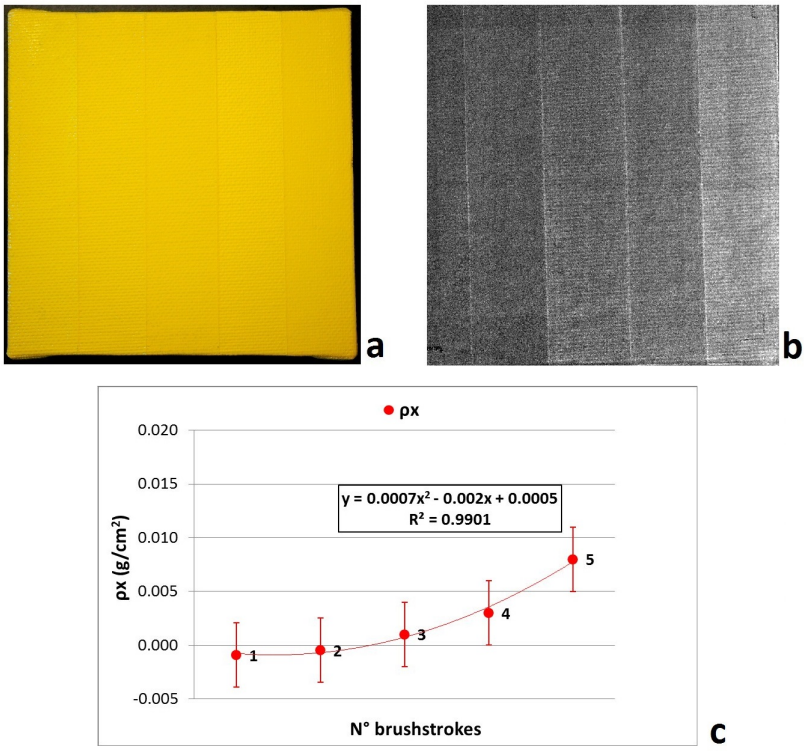

Figure 3.15: Lehmann image of cadmium yellow: a) color photo of the test object, b) Lehmann image, c) graph of the ρx of cadmium for each area (N° of brushstrokes). RX acquired at 35 kV, 60 mA, 1.55 mm Al, 1s, Mo anode.

Table 3.2: Equivalent material for Cadmium yellow canvas and corresponding μ/ρ

Material	**Energy (keV)**	μ/ρ **(cm^2/g)**
PMMA	26.1	~ 0.36
	27.3	~ 0.34

Cadmium red

The **cadmium red** canvas also shows a behaviour similar to the KES image. In Figure 3.16, the Lehmann image and the relative ρx are displayed (b and c). Again, the section 2 is as light as section 4 and the same amount of Cd is revealed (c).

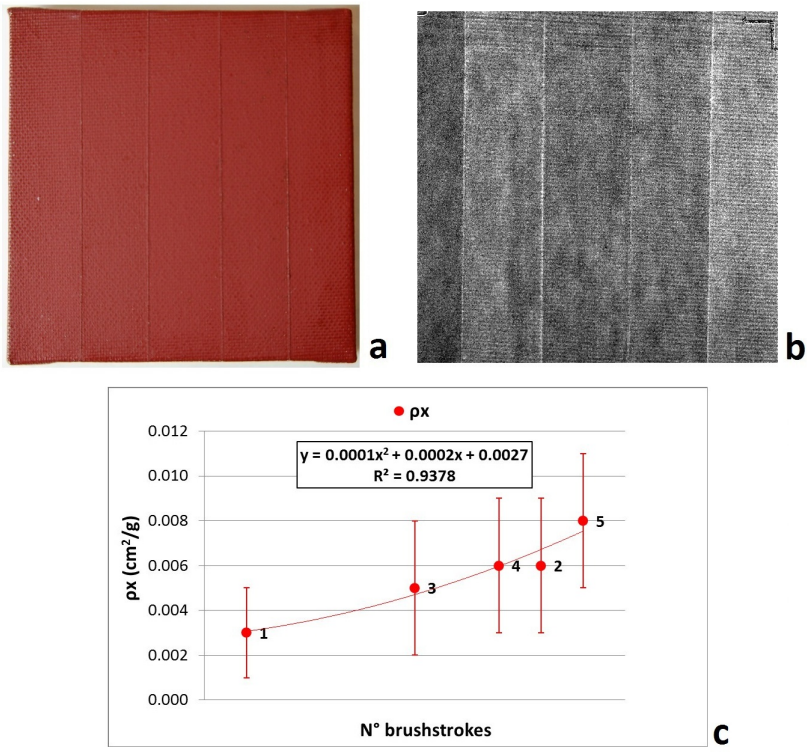

Figure 3.16: Lehmann image of cadmium red: a) color photo of the test object, b) Lehmann image, c) graph of the ρx of cadmium for each area (N° of brushstrokes). RX acquired at 35 kV, 60 mA, 1.55 mm Al, 1s, Mo anode.

Table 3.3: Equivalent material for Cadmium red canvas and corresponding μ/ρ

Material	**Energy (keV)**	μ/ρ **(cm^2/g)**
PMMA	26.1	~ 0.36
	27.3	~ 0.34

The Lehmann algorithm, at this point, follows the cps revealed by the XRF technique and the greylevels* of the KES images, so it is consistent with the other two techniques.

Overlapping pigments canvases

Considering the mock-ups with two pigments overlapping, a corrective factor (1.2) for the Cd image has been used to apply the KES processing. This correction has been maintained for the Lehmann Algorithm. Moreover, the most promising equivalent material for

the algorithm seemed to be the titanium white (TiO_2), which is in the preparation layer of the canvases.
The absorption coefficient used were 4.5 cm^2/g for the low energy and 3.7 cm^2/g for the high energy.

Naples and cadmium yellow

Starting from the **Naples and cadmium yellow** (Figure 3.17), the equivalent material used for the Lehmann Algorithm is Naples yellow, instead of titanium white. The lighter area in the resulting image (b) is where there is only cadmium yellow. Furthermore, the graph (c) shows positive values of ρx only for it, while, where there is the superposition of the two pigments, the value indicates that there is no cadmium, like in the left side of the canvas.

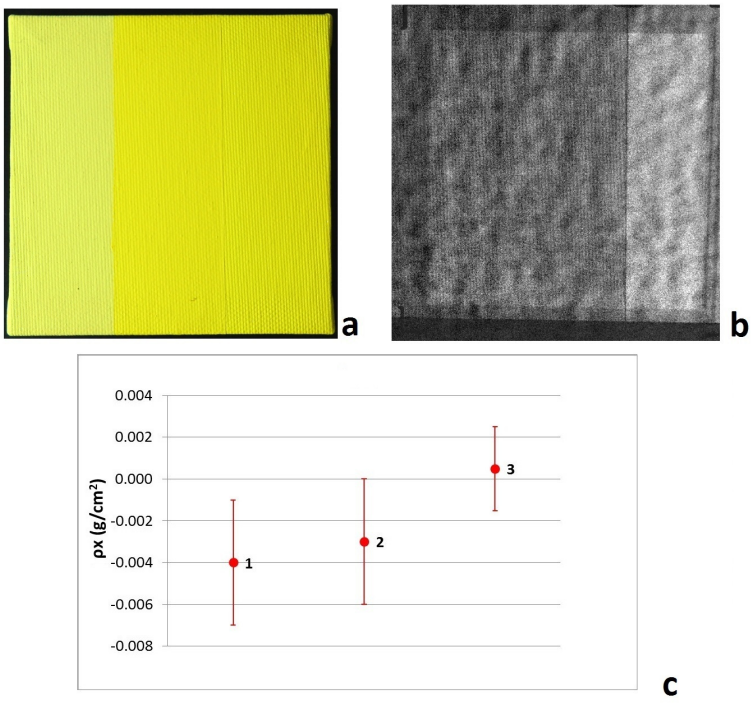

Figure 3.17: Lehmann image of Naples and cadmium yellow: a) color photo of the test object, b) Lehmann image, c) graph of the ρx of cadmium for each area. RX acquired at 35 kV, 60 mA, 1.55 mm Al, 1s, Mo anode.

Table 3.4: Equivalent material for Naples and cadmium yellow canvas and corresponding μ/ρ

Material	**Energy (keV)**	μ/ρ **(cm^2/g)**
Naples	26.1	$\sim$ 34.57
yellow	27.3	$\sim$ 24.45

Looking to the data reported in Figure 3.11, the result follows the same trend of the KES technique. Then, it can be supposed that the presence of lead is disturbing also the Lehmann analysis.

Naples yellow and cadmium red

The same considerations can be made for the **Naples yellow and cadmium red** canvas (Figure 3.18). The lighter area is the one containing only the Cd pigment, and the ρx is positive only there. While the central portion of the canvas is similar to the Naples yellow area both for the Lehmann image (b) and the values in the graph (c).

Comparing to the KES results (Figure 3.12), the trend is the same for both the techniques, so what has been hypothesized before seems to be valid.

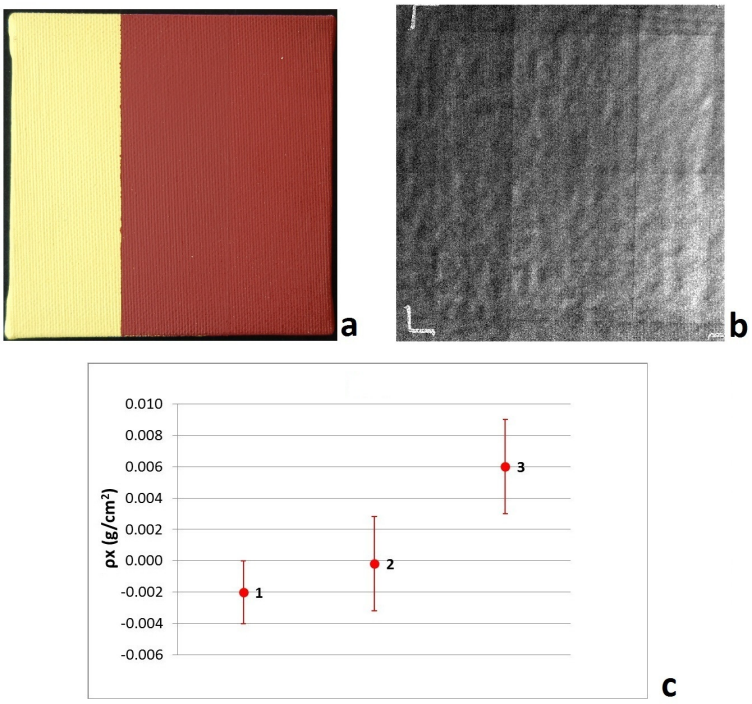

Figure 3.18: Lehmann image of Naples yellow and cadmium red : a) color photo of the test object, b) Lehmann image, c) graph of the ρx of cadmium for each area. RX acquired at 35 kV, 60 mA, 1.55 mm Al, 1s, Mo anode.

Table 3.5: Equivalent material for Naples yellow and cadmium red canvas and corresponding μ/ρ

Material	**Energy (keV)**	μ/ρ **(cm^2/g)**
titanium	26.1	~ 4.5
white	27.3	~ 3.7

Cadmium yellow and realgar

The last canvas analysed is the **cadmium yellow and realgar** (Figure 3.19). The resulting image (b) is really noisy, because to the low number of photons. The noise can be appreciated also in the big error lines reported in the graph (c). However, even if the result on the Cd yellow (left side of the mock-up) is consistent with zero (see the graph), it has a positive mean value and the trend of all the areas is the same of the KES elaboration (Figure 3.13).

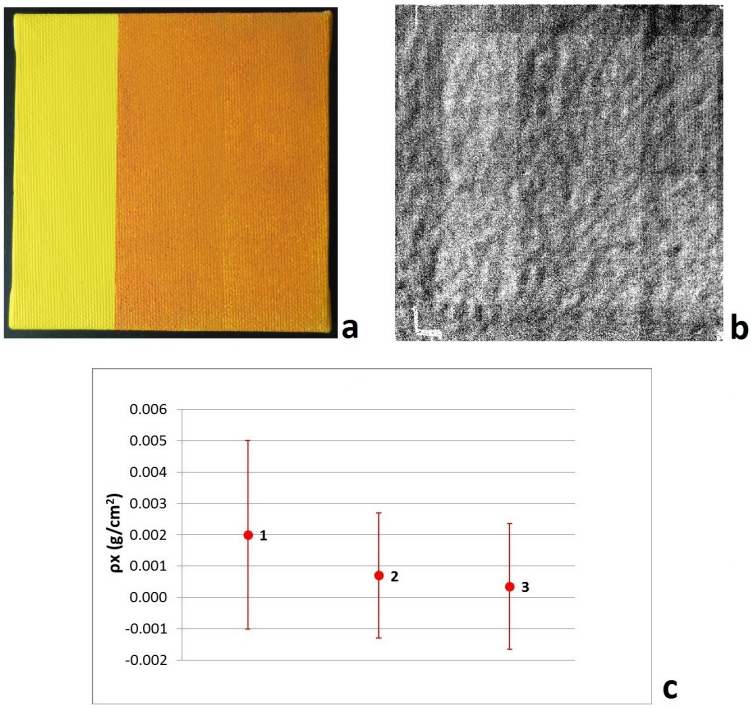

Figure 3.19: Lehmann image of cadmium yellow and realgar: a) color photo of the test object, b) Lehmann image, c) graph of the ρx of cadmium for each area. RX acquired at 35 kV, 60 mA, 1.55 mm Al, 1s, Mo anode.

Table 3.6: Equivalent material for cadmium yellow and realgar canvas and corresponding μ/ρ

Material	**Energy (keV)**	μ/ρ **(cm^2/g)**
titanium	26.1	~ 4.5
white	27.3	~ 3.7

Remembering that in this last canvas the pigment covering the Cd is with As and not with Pb, and considering that it hides the presence of cadmium also in the KES processing, it can be conclude that the presence of a medium/high Z element could cause the K-edge radiography to be inefficient.

3.1.3 Further tests

For cadmium, the doubt that the Mo anode fluorescence lines of the source are not equally attenuated by the three filters used (Ag, Cd, In), exists. For this reason, an additional test has been performed adding a copper filter 0.1 mm thick, in order to strongly attenuate the molybdenum lines. In Figure 3.20, the CZT spectra obtained are shown, and in the following one (Figure 3.21) the differences between them are reported (simulating virtual beams which could generate the Low and High Energy images). This figure shows that in the subtraction of the spectra the contribution of the Mo lines is no more significant.

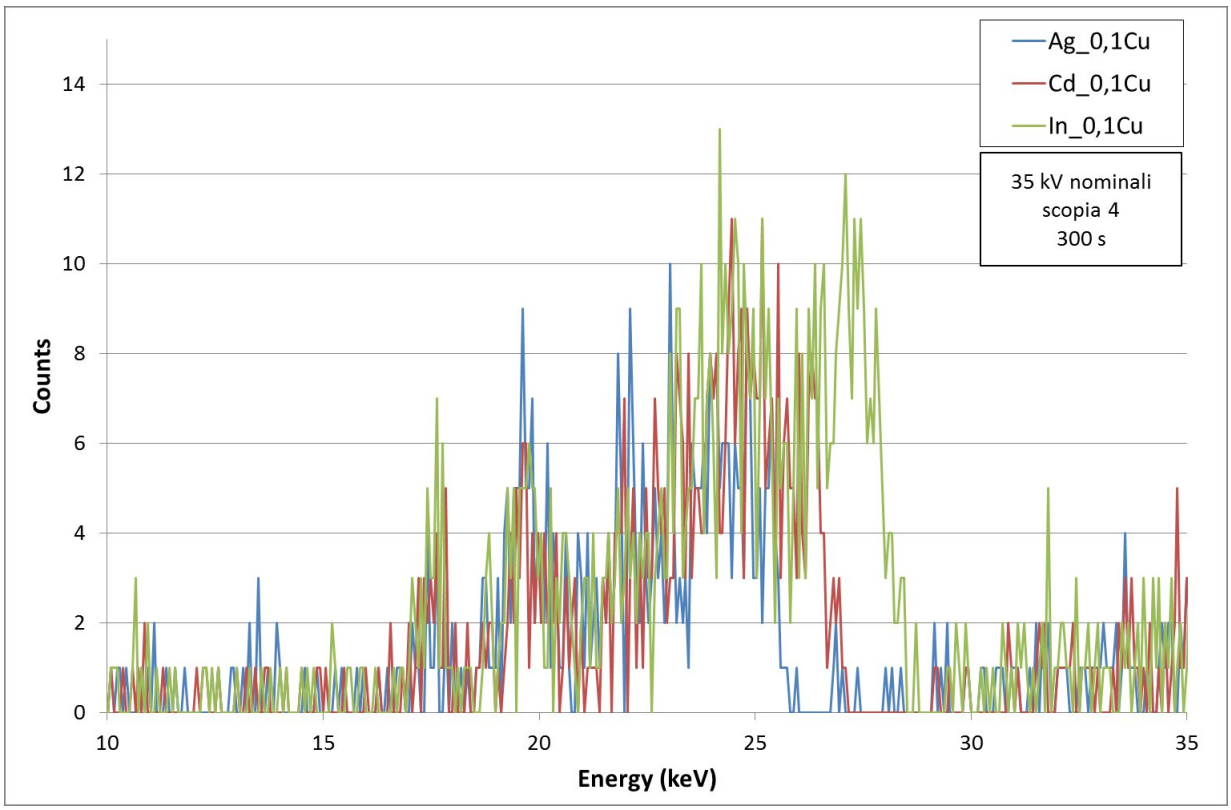

Figure 3.20: CZT spectra of the X-ray beam filtered by Ag, Cd and In filters and 0,1 mm Cu filter. The peaks at 17.4 and 19.9 keV are the fluorescence lines of the anode.

The copper filter attenuates also the energies around the K-edge of cadmium, so, testing the **Naples and cadmium yellow** sample, the current of the X-ray tube has been increased from 60 mA to 90 mA to guarantee enough photons.

The Figure 3.22 reports the results obtained: the KES (b) and Lehmann (c) images are less noisy and, in general, the greylevels* are higher than the previous test. However, where there is the overlapping of the pigments (area 2), the greylevels* in the graph d) are less then in the area 3, but higher than the Naple yellow part (area 1). In the graph e) the concentration of Cd seems to be higher than the old test, but again the area 2 (corresponding to the overlapping of the two pigments) seems to have a minor content of

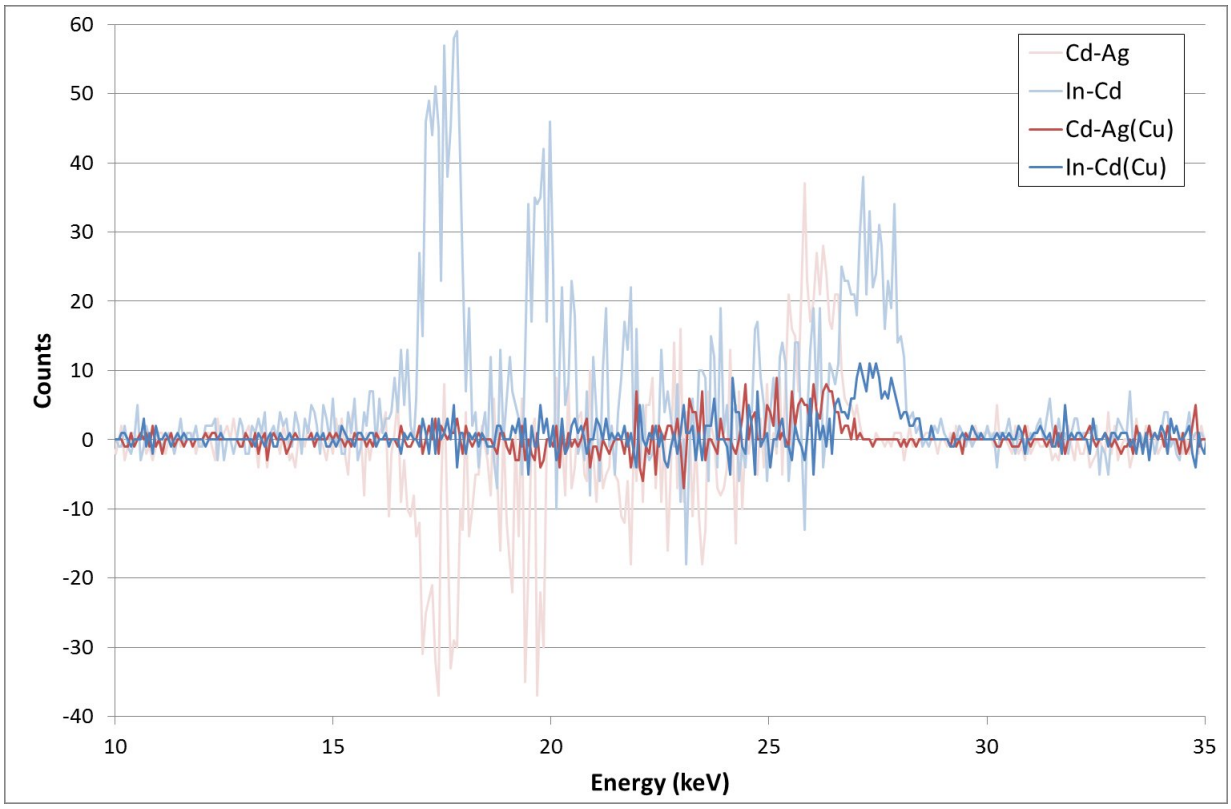

Figure 3.21: Differences between the spectra acquired with the Ag, Cd and In filters. For the darker colours the spectra have been acquired adding the copper filter.

Cd.

In general, these results are better than the previous, because of the higher greylevels* and the better discrimination of the 1^{st} and 2^{nd} areas.

Table 3.7: Equivalent material for Naples and cadmium yellow canvas and corresponding μ/ρ

Material	**Energy (keV)**	μ/ρ **(cm^2/g)**
Naples	26.1	$\sim$ 34.57
yellow	27.3	$\sim$ 24.45

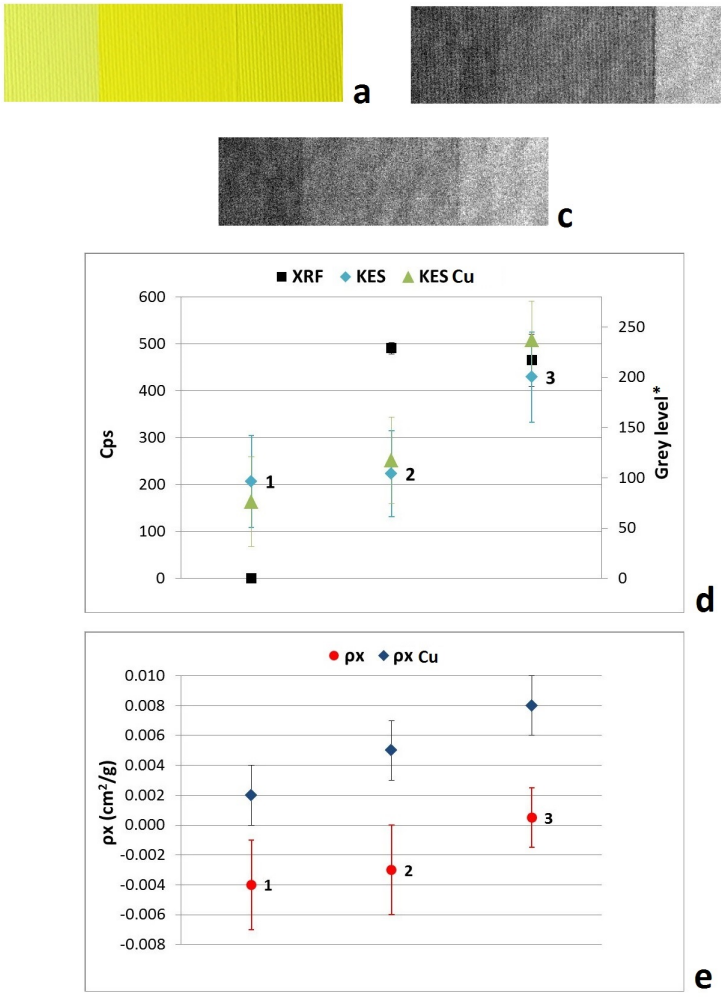

Figure 3.22: KES and Lehmann radiography of Naples and cadmium yellow: a) color photo of the test object: the Cd yellow is on the right side, b) KES image, c) Lehmann image, d) counts per second on Cd peak from the XRF analysis (50 kV, 700 μA, 60 s) and mean greylevel* for each area in green compared with the results of 3.11 (light blue), e) graph of the ρx of cadmium for each area in blue compared with the results of 3.17 in red. RX acquired at 38 kV, 90 mA, 0.1 mm Cu, 1.5 s, Mo anode

The same test has been repeated adding some metallic inserts, in order to have some references in the final images. They are a Cd foil 38.7 μm thick, 15 foils of Al and a small Al washer. In the Figure 3.23, the results for the KES elaboration are reported.

Looking at the image b), the Al foils and the washer are darker than all the other materials, while the Cd foil is the lighter one, confirming that the KES technique works properly. C) is the same image, where the contrast has been enhanced for the Cd foil. As result, the cadmium yellow area is enhanced too.

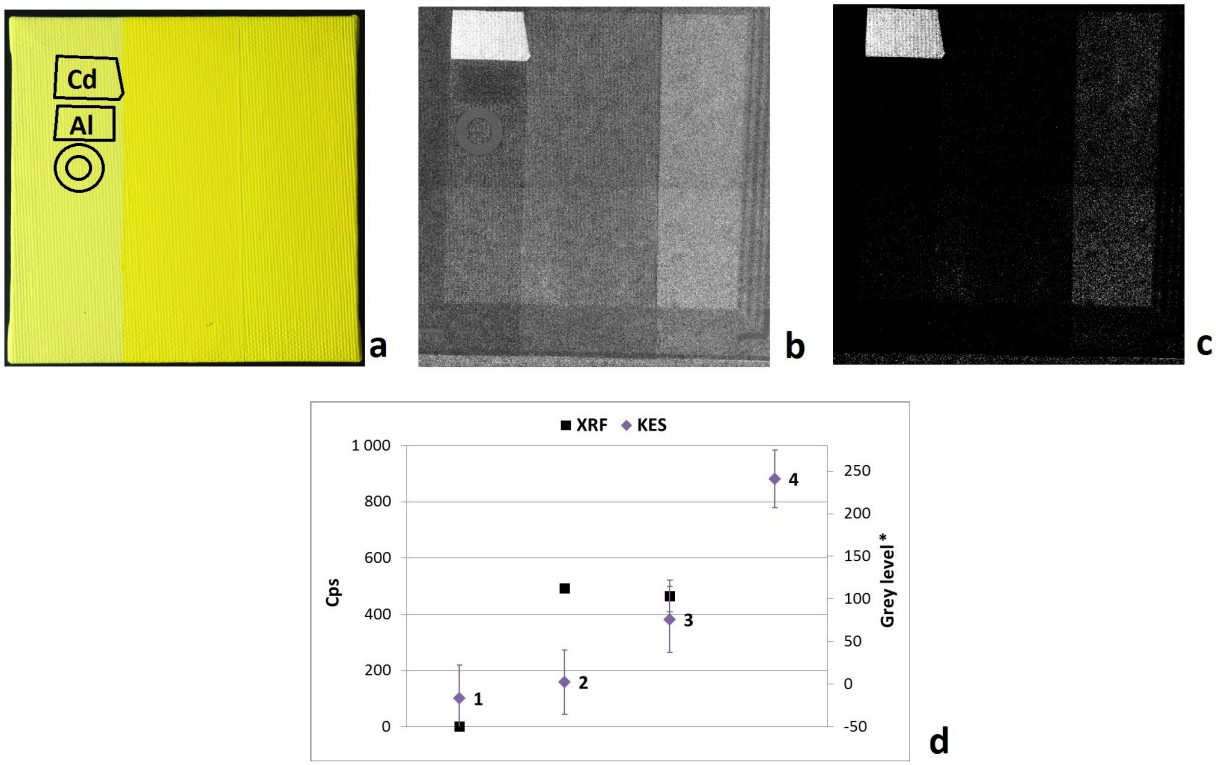

Figure 3.23: KES radiography of Naples and cadmium yellow: a) color photo of the test object with the position of the metallic inserts: the Cd Yellow is on the right side, b) KES image, c) contrasted KES image, d) counts per second on Cd peak from the XRF analysis (50 kV, 700 μA, 60 s) and mean greylevel* for each area (4 stands for the Cd foil). RX acquired at 38 kV, 90 mA, 0.1 mm Cu, 1.5 s, Mo anode

About the elaboration with the Lehmann Algorithm (Figure 3.24), in the image referring to the presence of Cd (b), not only the metallic foil is lighter, but also the washer and the frame clips.

However, looking at the image c), which is the image referring to all the materials that are not cadmium, these metallic elements are really bright, the foils of Al are visible and the cadmium target has vanished. The interpretation of these two images indicates that only the Cd foil and the right area of the sample (cadmium yellow) give a positive response to

the algorithm.

In the graph d), the content of Cd of the metallic foil (4) is really high, compared with the zone with only cadmium yellow (3). It could indicate that the thickness of the target is too high for a comparison with real painted layers, and a thinner foil or another kind of target should be considered.

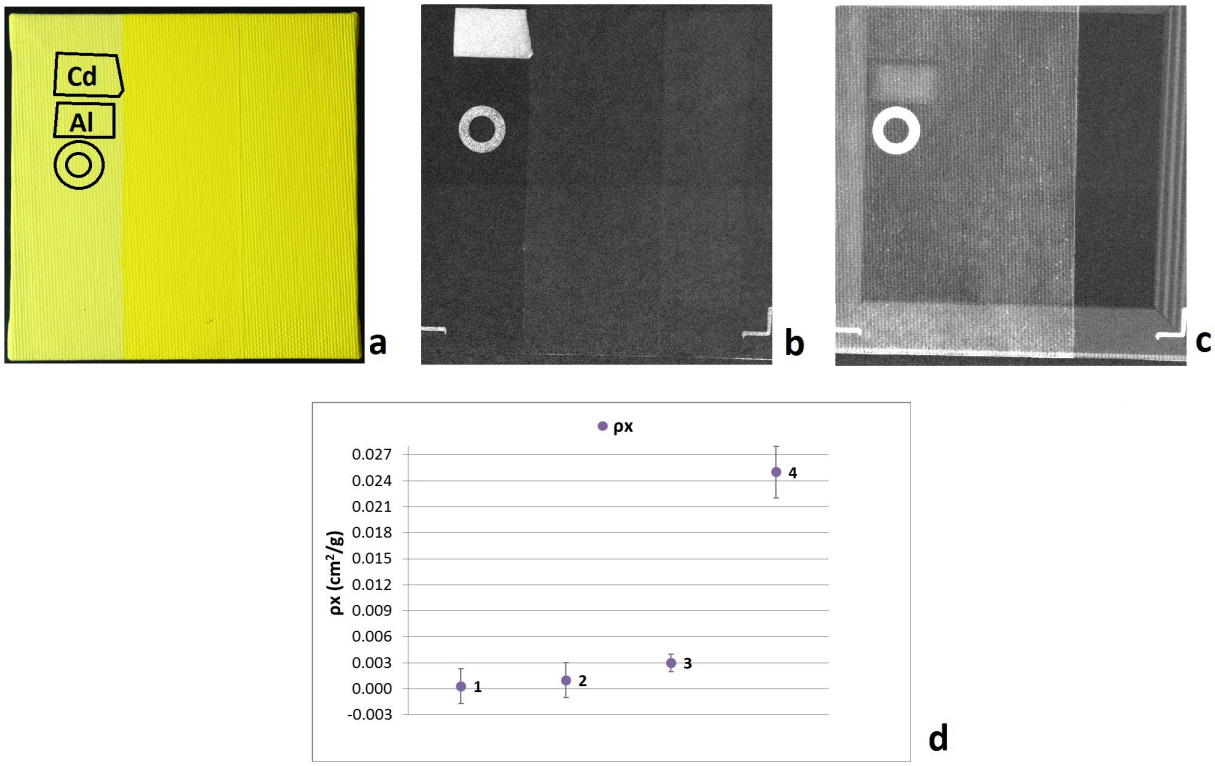

Figure 3.24: Lehmann radiography of Naples and cadmium yellow: a) color photo of the test object with the position of the metallic inserts: the Cd Yellow is on the right side, b) Lehmann image of Cd, c) Lehmann image of other elements, d) graph of the ρx of cadmium for each area. RX acquired at 38 kV, 90 mA, 0.1 mm Cu, 1.5 s, Mo anode

Table 3.8: Equivalent material for Naples and cadmium yellow canvas and corresponding μ/ρ

Material	**Energy (keV)**	μ/ρ **(cm^2/g)**
Naples	26.1	$\sim$ 34.57
yellow	27.3	$\sim$ 24.45

3.1.4 Conclusion

To summarize, considering the gradation of the cadmium pigments canvases, the KES and Lehmann algorithm elaborations give results near the limit of non-sensitivity for the first two brushstrokes. Looking at the XRF analysis, they correspond to values between 200 and 600 cps. So, when the response to the XRF is under 600 cps, the K-edge radiography using balanced filters is not sensitive.

Furthermore, the presence of layers with other elements limits even more the detectability of the cadmium, whether applying the KES elaboration or the Lehmann algorithm.

In the last tests performed, the addition of a copper filter and the increasing of the tube current give better results.
At the moment, if a known target of cadmium is not present in the images, the K-edge radiography with balanced filters seems not to be a good elemental imaging technique, due to its very low sensitivity.

3.2 Copper and Cobalt

In the test canvas for copper and cobalt the pigments employed have been mixed with rabbit glue. The pigments used for the copper are azurite[8] (copper hydroxide carbonate, $2CuCO_3Cu(OH)_2$) and malachite[9] (copper hydroxide carbonate, $2CuCO_3Cu(OH)_2$), for cobalt they are cobalt bottle green[10] (cobalt chromite green spinel, $CoCr_2O_4$) and cobalt blue[11] (cobalt zinc silicate, $(Co,Zn)_2SiO_4$).

In Figure 3.25, the test mock-ups are reported: there are the scales (from 1 to 5 brush-strokes) of all the four pigments used, and two overlapping samples. In the first, azurite and cobalt blue are superposed, in the second malachite and cobalt green.

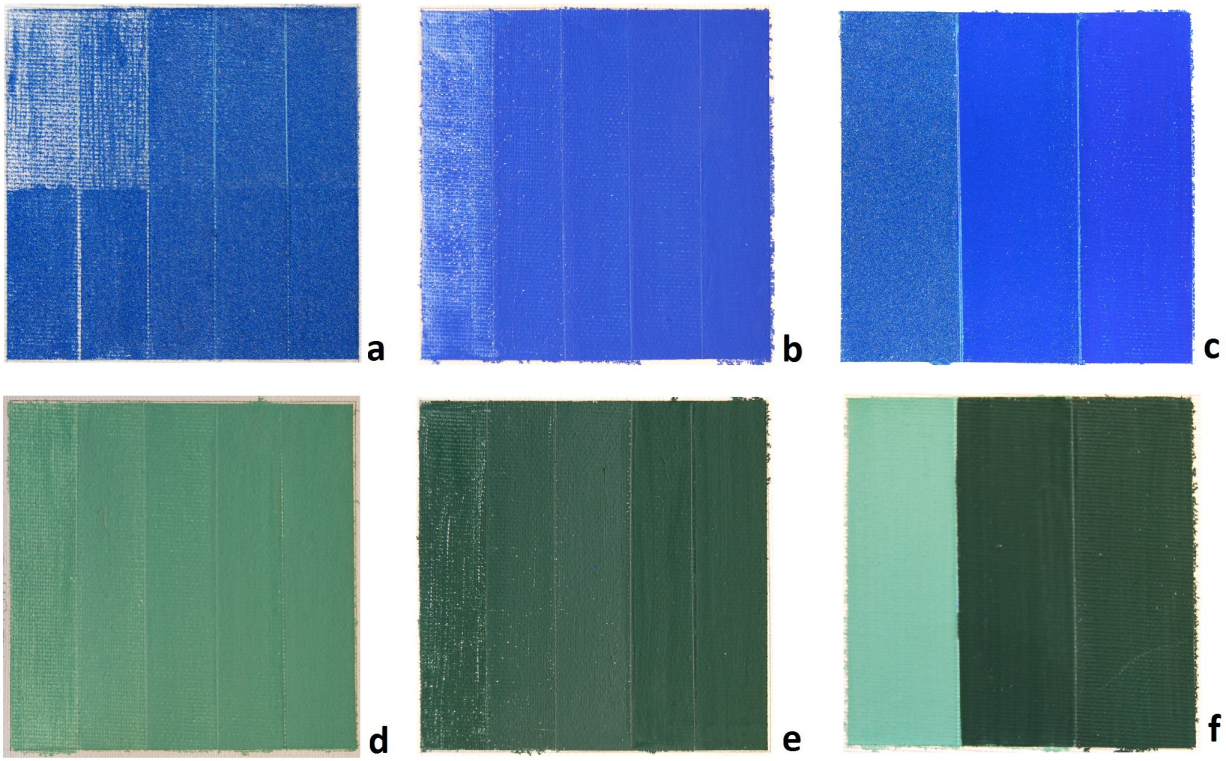

Figure 3.25: Cu and Co test objects: a) azurite scale, b) cobalt blue scale, c) overlapping of azurite and cobalt blue, d) malachite scale, e) cobalt green scale, f) overlapping of malachite and cobalt green

[8] n° 10203, Kremer
[9] n° 10300, Kremer
[10] n° 44130, Kremer
[11] n° 45700, Kremer

3.2.1 KES technique

About the K-Edge Subtraction (KES) technique, for all the Cu tests, three radiographies have been acquired with the filters of nickel, copper and zinc. The elaboration has been made subtracting the Ni image from the Cu one, in order to obtain the Low Energy image, and the Cu image from the Zn one, obtaining the High Energy image.

Azurite

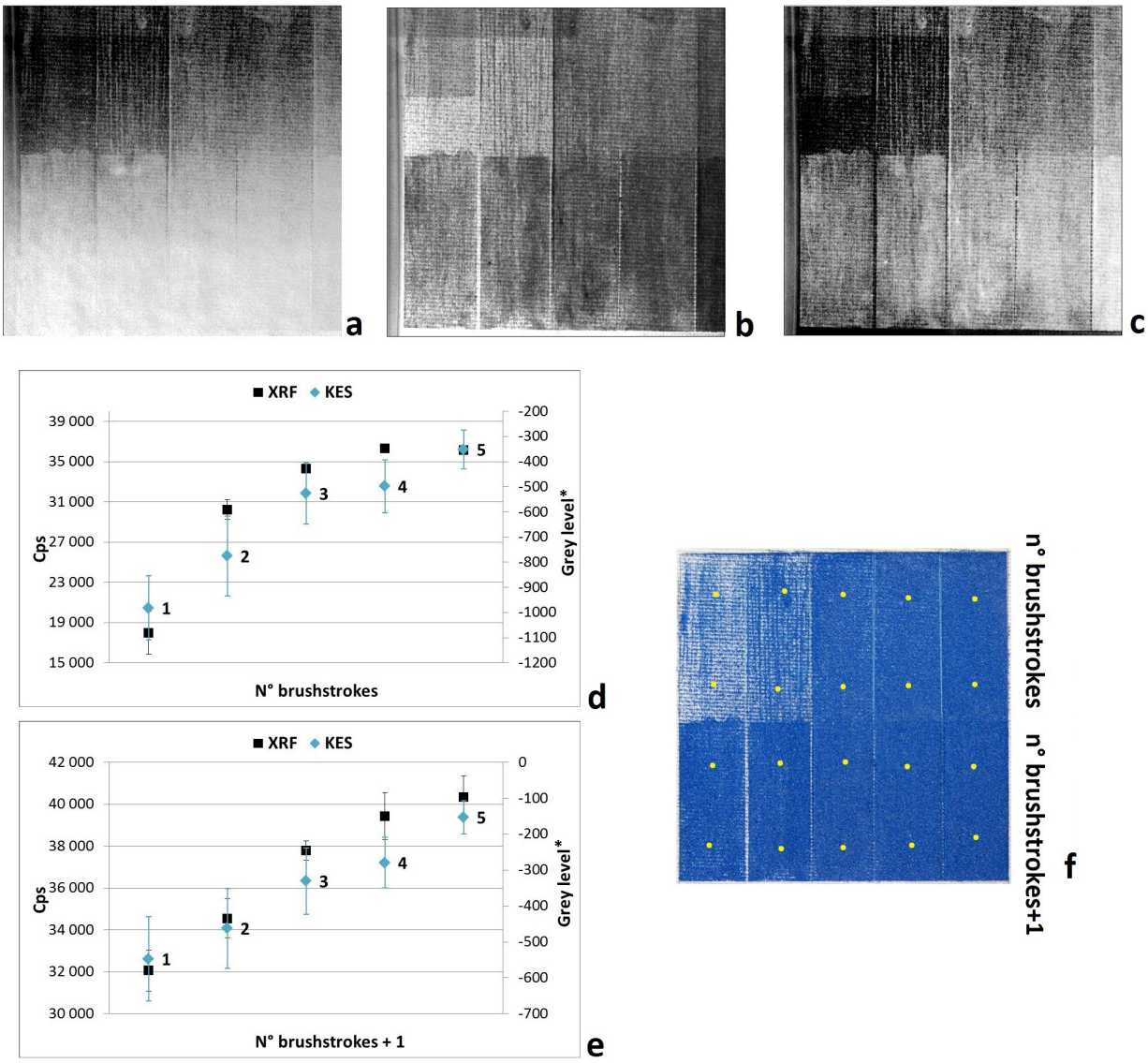

Figure 3.26: KES radiography of azurite: a) Low Energy image, b) High Energy image, c) KES image, d) counts per second on Cu peak from the XRF analysis (50 kV, 700 μA, 60 s) and mean greylevel* for each area (N° of brushstrokes) for the upper section, e) graph of the lower section, f) color photo of the test object with the XRF spots (yellow). RX acquired at 20 kV, 60 mA, 2.5 s, Mo andode.

Starting from the **azurite** sample (Figure 3.26), it is composed of two sections which are

different only because in the lower part one more brushstroke has been applied (f). The first image a is the Low energy image, b) is the High energy image and c) is the resulting subtraction (KES image), in which lighter areas indicate a bigger amount of copper.

In the graphs d) and e), the counts per second (from the XRF analysis) increase as the number of brushstrokes increases, except for the the area 5 in the upper section, which is similar to the 4 (d). However, looking at the greylevels*, the area 4 is more similar to the 3 than to the 5. It could depend on the XRF points chosen.

Malachite

In Figure 3.27, the results of the KES and XRF techniques for the **malachite** test are shown. The lighter area in the KES image (c) correspond to an higher content of copper (neglecting the areas with wood, in the down-left corner).

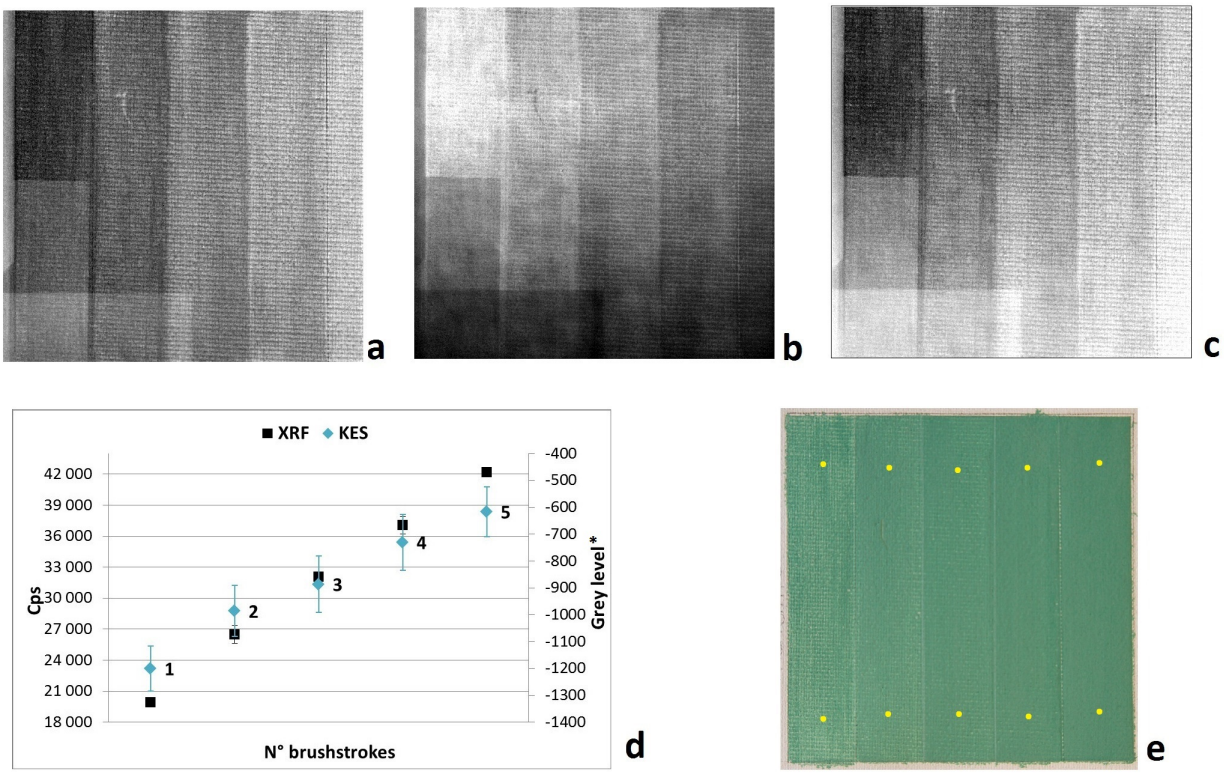

Figure 3.27: KES radiography of malachite: a) Low Energy image, b) High Energy image, c) KES image, d) counts per second on Cu peak from the XRF analysis (50 kV, 700 μA, 60 s) and mean greylevel* for each area (N° of brushstrokes), e) color photo of the test object with the XRF spots (yellow). RX acquired at 20 kV, 60 mA, 2.5 s, Mo andode.

Coming to the graph d), in this case the linearity between the cps and the amount of

copper is maintained and also the greylevels* are following it. Furthermore, there is a good separation between the greylevels* of the 5 areas, due to more marked differences in the content of Cu among the brushstrokes.

Looking at the fit of the two copper samples (Figure 3.28), a strong linearity between the number of brushstrokes, then the amount of Cu, and the KES result for each area is highlighted. Furthermore, the linearity increases when a bigger amount of copper is present, as it is evident in the azurite graph (a) for the area painted with one more layer (KES+1).

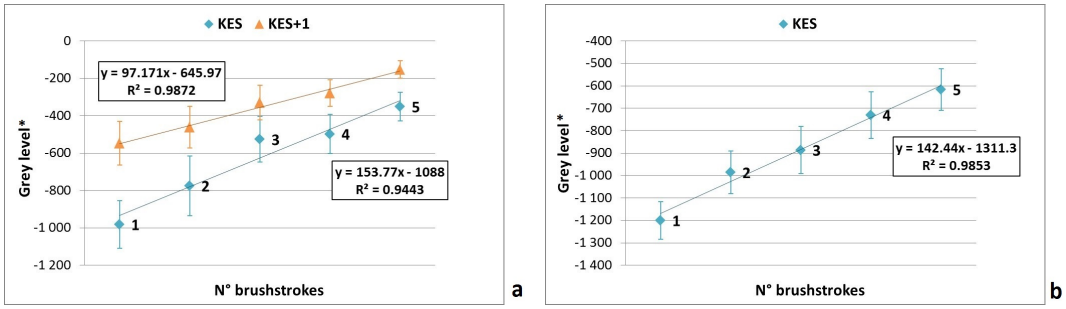

Figure 3.28: Fit of the greylevel* measured for the azurite canvas (a) in the two areas (KES and KES+1) and the malachite canvas (b).

Cobalt blue

Concerning the cobalt radiographies, three images have been acquired with the filters of iron, cobalt and nickel. The elaboration has been made subtracting the Fe image from the Co one (Low energy image) and the Co image from the Ni one (High energy image). Working in these conditions, the results obtained for the cobalt blue and the cobalt green are contrasting. For the first the KES elaboration failed, while for the cobalt green it worked properly.

In Figure 3.29, the KES image c) for the **cobalt blue** pigment is lighter in the left side and darker in the right one, even if the major amount of Co is on the right. The parameters set for acquiring the three radiographies may be not the best for this element, or the content of cobalt is not enough and is under the minimum detectable limit for this technique.

In the graph d) the cps revealed by the XRF technique are reported. It could indicate that XRF is more sensible to small quantities of elements (for example, cobalt), if they are on the surface, than the K-Edge radiography.

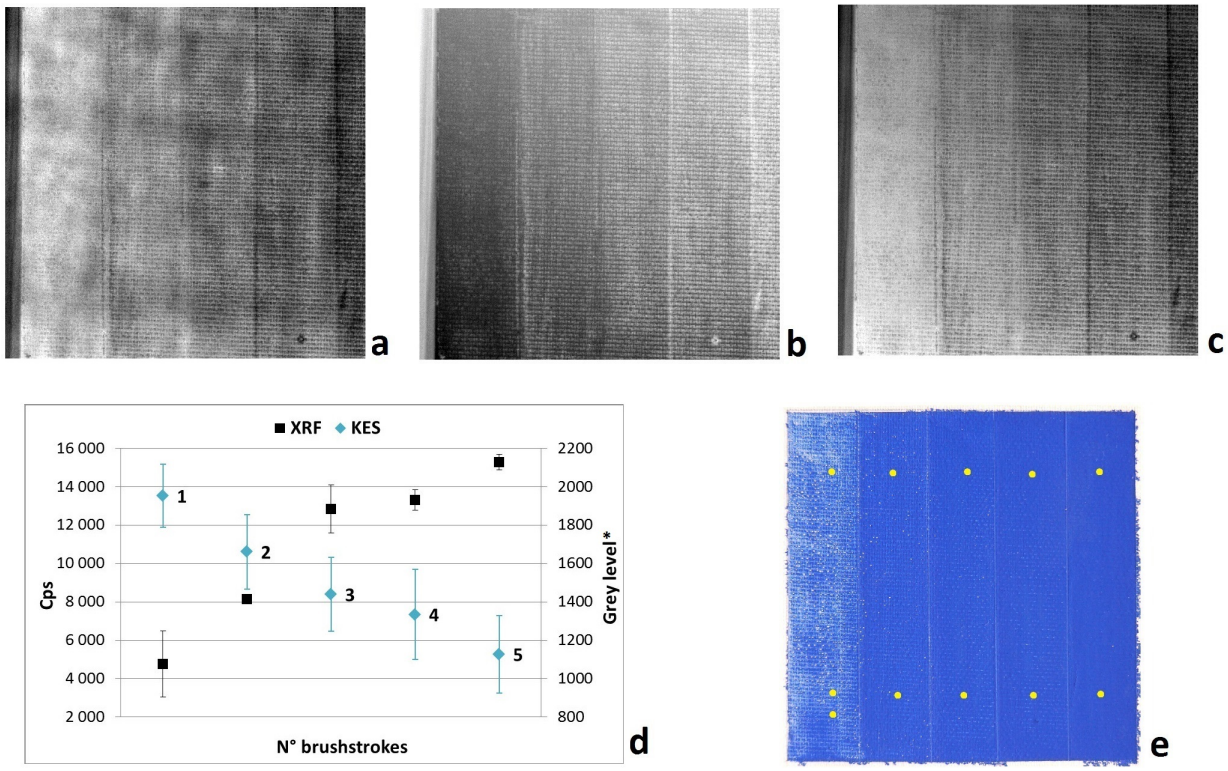

Figure 3.29: KES radiography of cobalt blue: a) Low Energy image, b) High Energy image, c) KES image, d) counts per second on Co peak from the XRF analysis (50 kV, 700 μA, 60 s) and mean greylevel* for each area (N° of brushstrokes), e) color photo of the test object with the XRF spots (yellow). RX acquired at 20 kV, 19 mA, 2.5 s, Mo anode.

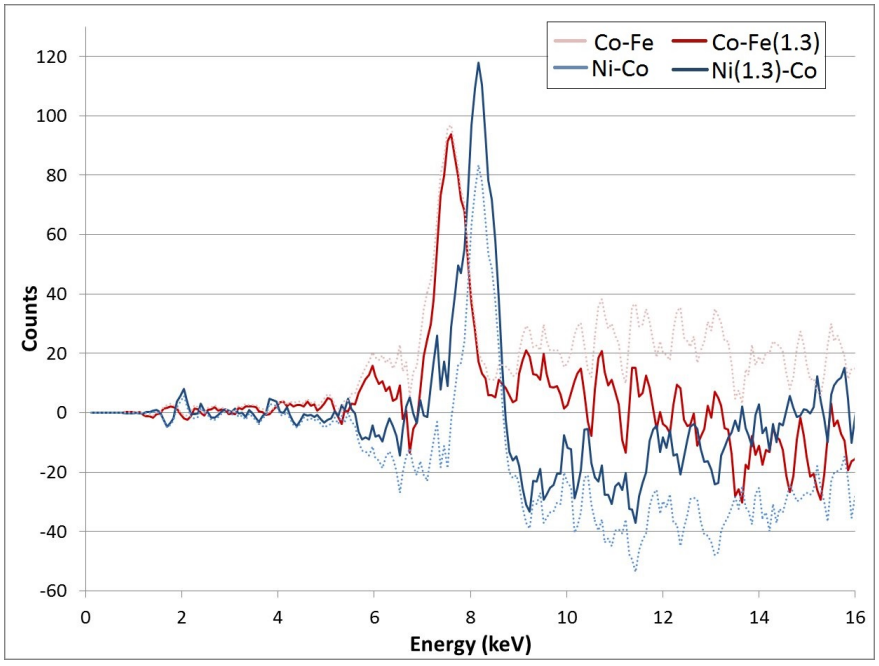

Figure 3.30: Differences between the spectra acquired with the Fe, Co and Ni filters. For the darker colours the Fe and Ni spectra have been multiplied for 1.3

Cobalt green

For the **cobalt green** sample, the KES technique seems to be more promising. During the elaboration of the images, the iron and nickel images have been multiplied for 1.3 as corrective factor.

As can be seen in Figure 3.30, the differences between the spectra acquired with the Fe, Co and Ni filters simulate a virtual beam which could generate the Low and the High Energy images. The principal effect of the two corrective factor is to equalize the two spectra for the energies over 10 keV. Furthermore, the High energy spectrum (Ni-Co) is increased.

In Figure 3.31, the results for the KES elaboration, applying the two factors to the iron and nickel images, are presented. The resulting image (c) is lighter in the right side, where 5 brushstrokes have been painted.

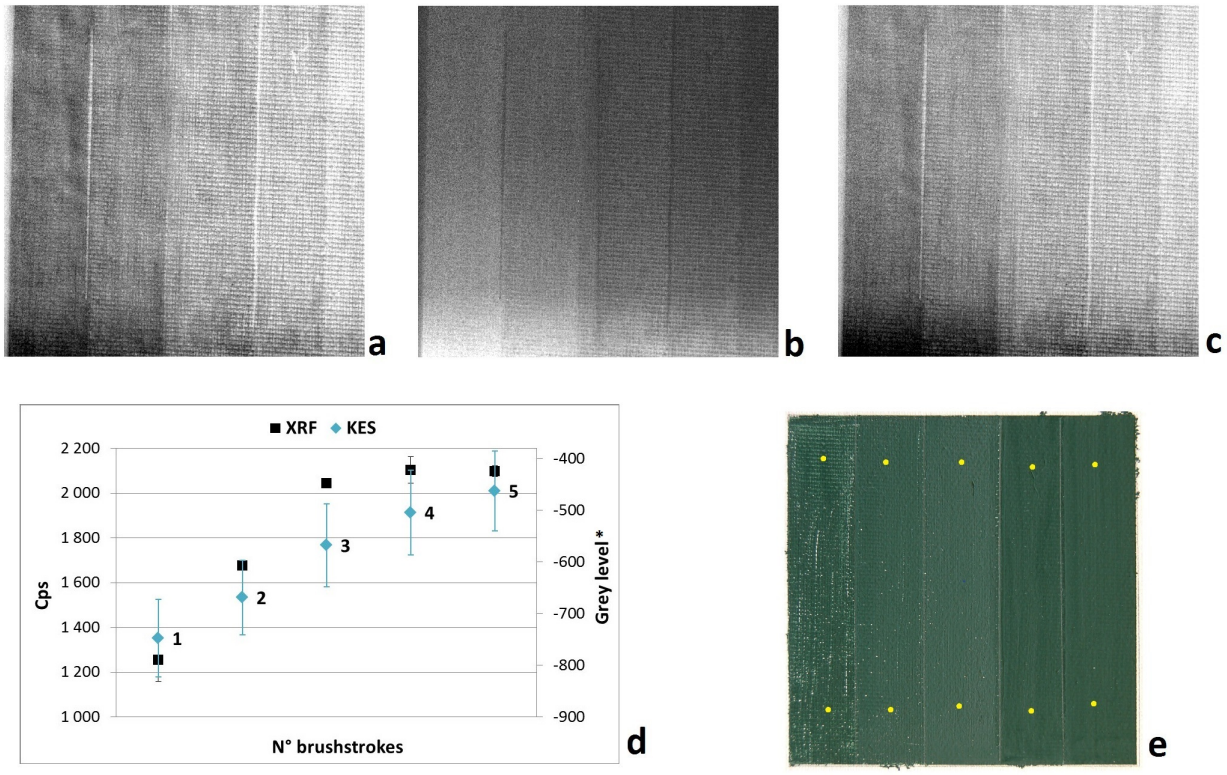

Figure 3.31: KES radiography of cobalt bottle green: a) Low Energy image, b) High Energy image, c) KES image, d) counts per second on Co peak from the XRF analysis (50 kV, 700 μA, 60 s) and mean greylevel* for each area(N° of brushstrokes), e) color photo of the test object with the XRF spots (yellow). RX acquired at 20 kV, 19 mA, 2.5 s, Mo anode.

From the cps of the graph d, the area 3, 4 and 5 seems to be very similar in the quantity of cobalt. About the greylevels*, even if the three measured areas are consistent between

them, the KES technique seems to better separate them.

In this last case, referring to the graph in Figure 3.32, a very good linearity in the greylevel* has been found, respect to the XRF results.

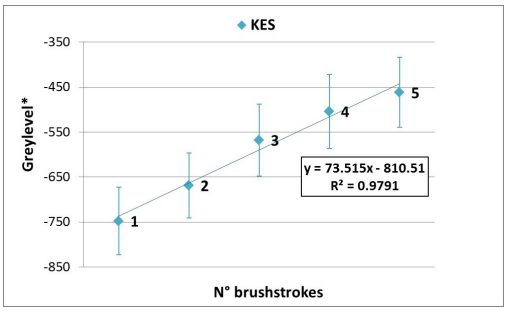

Figure 3.32: Fit of the greylevel* measured for the cobalt green canvas.

Azurite and cobalt blue

For the blue overlapping sample (e in Figure 3.33), **azurite** has been painted on the left side and **cobalt blue** on the right one. In the central area, azurite is covered by cobalt blue. Starting with the elaboration of copper, the KES image is light in the left and central area, and dark in the right one, which corresponds to the absence of copper. Furthermore, the greylevels* for the two areas with copper are the same in the graph d).

However, the XRF analysis (graph d) seems to indicate that in the central area the content of copper is less. This is due to the fact that azurite is under the cobalt blue layer, which may absorb the fluorescence X-rays of copper ($E_{K\alpha} = 8.05$ keV). The K-edge radiography reveals the presence of a target element through all the thickness of the sample, while the XRF technique is limited to the surface analysis.

On the contrary, looking at the cobalt results, the KES image (h) is lighter only in the right side, where there is only the cobalt blue pigment, while the central part is darker. The presence of another pigment works like a mask for the cobalt. In this case, it is due to the presence of heavier elements than Co in the same area.

The XRF cps are the same for the central and the right side of the sample, because the Co pigment is the upper one. XRF is a surface technique and fails to reveal copper underneath.

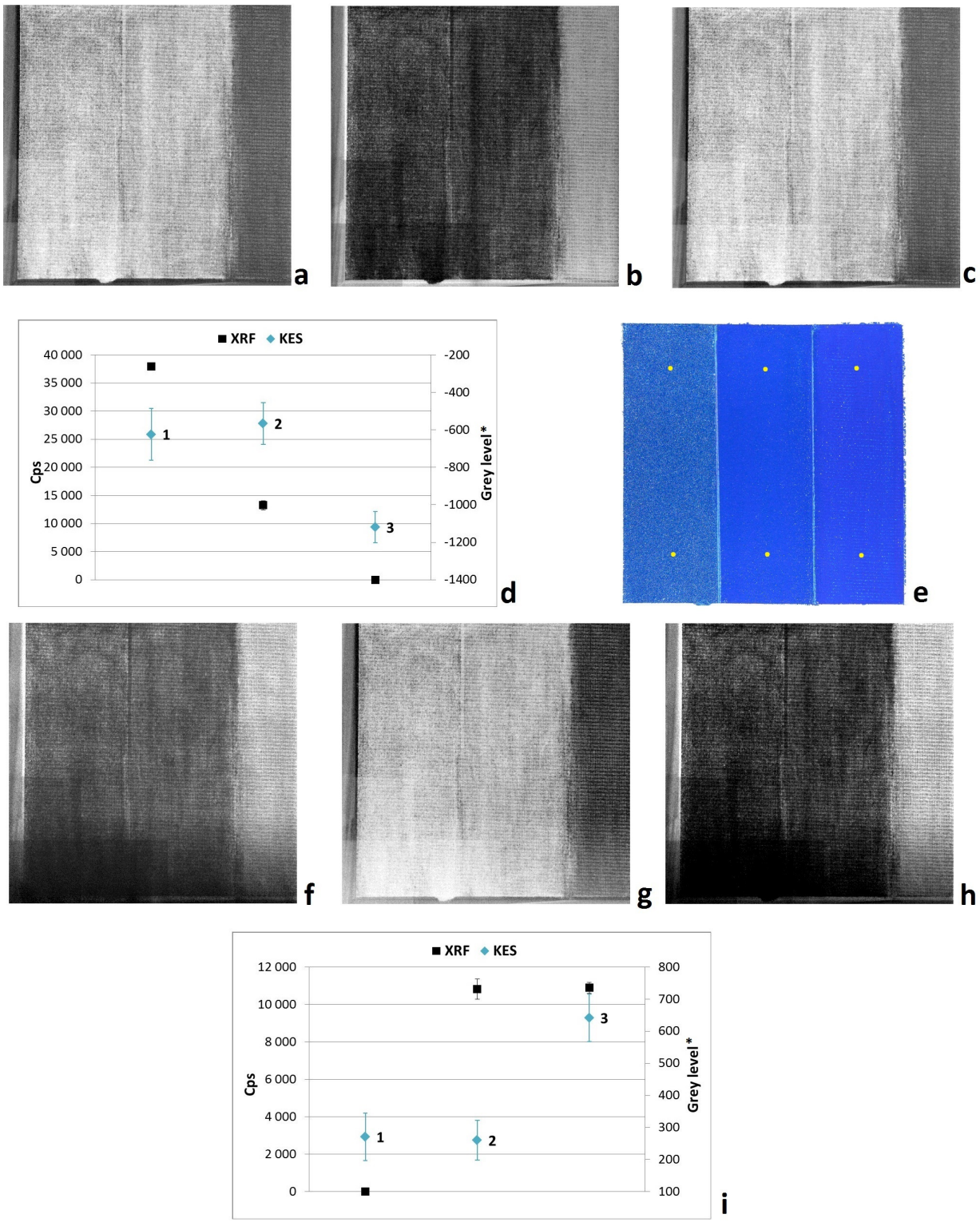

Figure 3.33: KES radiography of azurite and cobalt blue mock-up: a) Cu Low Energy image, b) Cu High Energy image, c) Cu KES image, d)counts per second on Cu peak from the XRF analysis (50 kV, 700 μA, 60 s) and mean greylevel* for each area, e) color photo of the Cu-Co test object with the XRF spots (yellow). RX acquired at 20 kV, 60 mA, 2.5 s, Mo anode.
f) Co Low Energy image, g) Co High Energy image, h) Co KES image, i)counts per second on Co peak from the XRF analysis (50 kV, 700 μA, 60 s) and mean greylevel* for each area. RX acquired at 20 kV, 19 mA, 2.5 s, Mo anode.

Malachite and cobalt green

The green overlapping test object (e in Figure 3.34) presents in the left side **malachite**, in the right side **cobalt green** and in the central area the superposition of the two pigments. As in the previous case, the cobalt pigment is over the copper one. Starting with the analysis of copper, even in this case, the KES image (c) indicates its presence in the left and central area of the sample. The right side is darker because of the absence of Cu.

Looking the graph d), the XRF highlights a small presence of copper in the central portion respect the left side. This is due to the superposition of the cobalt pigment layer that absorbs the Cu fluorescence X-rays.

Referring to cobalt, the KES image (h) is lighter in the right side, where the only cobalt Green has been painted, and darker in the other two areas. However, the central area is a little bit lighter than the left one. So, in this sample, even if cobalt is heavily masked by Malachite, it is weakly visible.

Considering the cps in graph i), in the central part it seems to be an higher amount of Co than the right part. This may affect the KES result. In fact, it could be that the limit detectable quantity of the K-edge radiography changes drastically in function of the other elements present. In this case, to highlight the presence of cobalt, when there is also malachite, a bigger amount of Co is needed than when only the target element is present. The presence of other elements works as a mask for the target one.

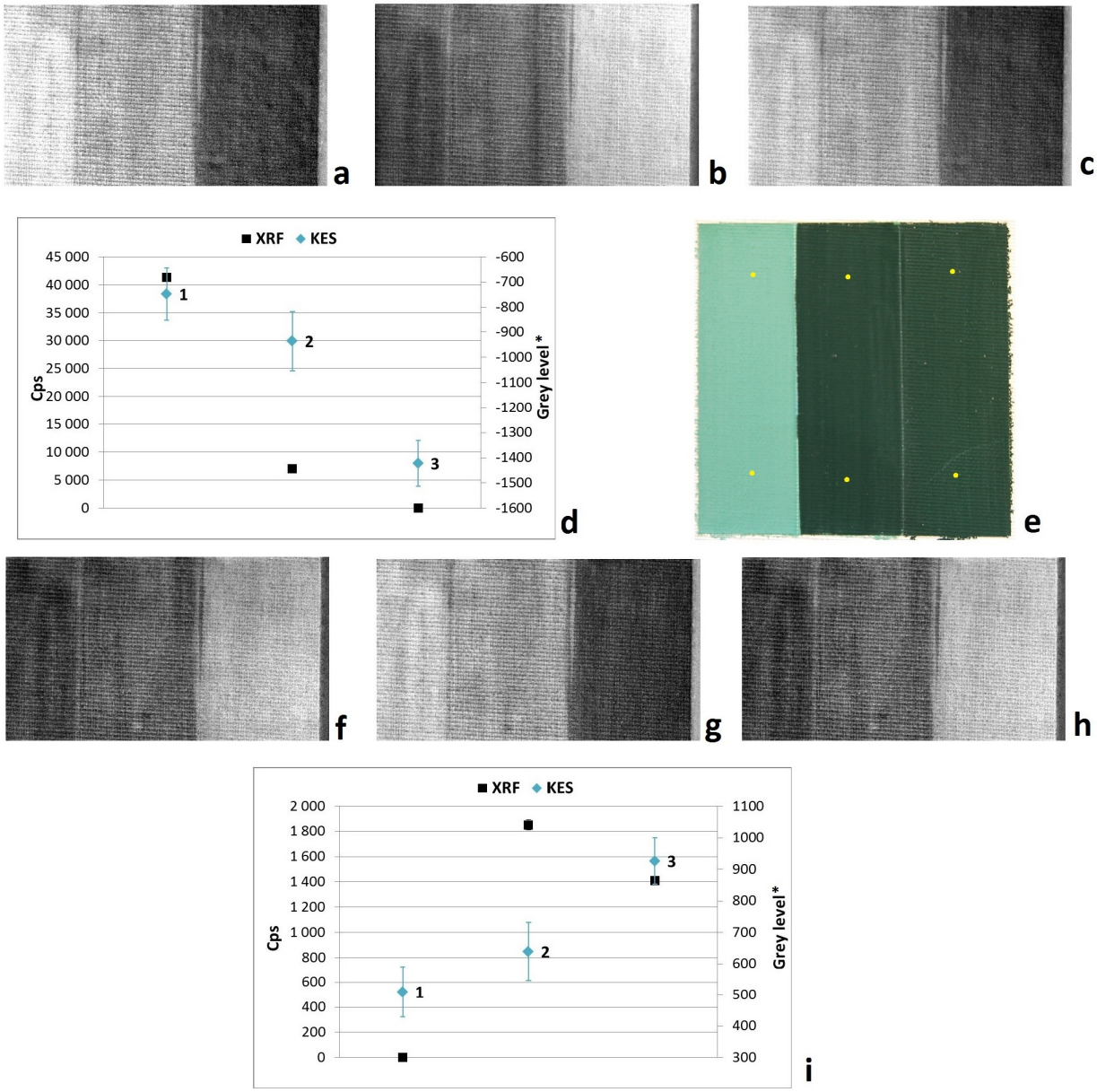

Figure 3.34: KES radiography of Malachite and cobalt Green mock-up: a) Cu Low Energy image, b) Cu High Energy image, c) Cu KES image, d)counts per second on Cu peak from the XRF analysis (50 kV, 700 μA, 60 s) and mean greylevel* for each area, e) color photo of the Cu-Co test object with the XRF spots (yellow). RX acquired at 20 kV, 60 mA, 2.5 s, Mo anode.
f) Co Low Energy image, g) Co High Energy image, h) Co KES image, i)counts per second on Cu peak from the XRF analysis (50 kV, 700 μA, 60 s) and mean greylevel* for each area. RX acquired at 20 kV, 19 mA, 2.5 s, Mo anode.

3.3 Conclusion

Considering the results obtained for the K-edge Radiography using balanced filters, it cannot be fully considered an elemental imaging technique, due to the fact that the detection of the target element strongly depends by the presence of the other elements or different thickness.

The other elements can act as a mask for the target, which is no more detectable, or attenuate its response. So, the final image cannot be considered a faithful representation of the target element map.

Conclusion

In this work two ways to obtain the K-edge radiography using common X-ray tubes have been investigated. The first, concerning the monochromatization of the X-ray beam via Bragg diffraction, is still carrying on for portability engineering.

The second way for the K-edge radiography using X-ray tubes is exploiting the differences among three images acquired with balanced filters. The target elements examined are cadmium, copper and cobalt.

After having investigated the beams filtered with the corresponding filters, some mock-ups painted with common pigments have been tested. The results, discussed in the 3^{rd} chapter, indicate that the presence of other materials strongly affects the final image. They could act as a mask for the target element and make the technique less sensitive. However, it is important to stress that their position, in the stratigraphy of the painting, is immaterial for the final result. Comparing with XRF, whose results are strongly affected by the surface composition, it is a significant advantage.

Finally, it seems to be essential an insert of a target element, which makes the measurements reproducible and reliable.

Appendix A

From X-radiography to Art History

Some cases studied analysed at the Laboratory of Archaeometry (Dept. of Physics and Earth science, University of Ferrara) by means of radiography, will be presented. They are paintings from the XV to the XX century, on wood and on canvas, and referring to different Italian schools.

Digital Radiographies have been performed *in situ* or at the laboratory of Ferrara University, using one of the scanners.

XV century: Virgin Mary in throne with the Child

The first painting is a wood panel with dimensions of 129 x 64 cm, representing the "Virgin Mary in throne with the Child" (Figure A.1). It is a painting of XV century, belonging to the Sicilian school.
The radiographies have been acquired at the Civic Gallery of Palazzo Bellomo in Siracuse (Sicily), using the new radiographic scanner.

From the radiography (Figure A.2), some typical element of the painting with golden background are highlighted, such as the border of the painted areas with the golden ones marked with a pigment containing a high Z element (probably Lead White), more evident in the face of the Virgin Mary.

The main peculiarity has been the discovering of fibres in the more fragile areas of the painting, such as the conjunction between the wood tables or the presence of knots. In b) Figure A.2, the radiographic detail of the Child is shown. The darker lines are the fibres mixed in the preparation to dampen the stress on the pictorial layer, instead of the use of a small piece of canvas. The peculiarity lays in the rarity on finding this technique.

Figure A.1: Anonymous, *Virgin Mary in throne with the Child*, XV century, wood, 129 x 64 cm, Siracuse, Palazzo Bellomo

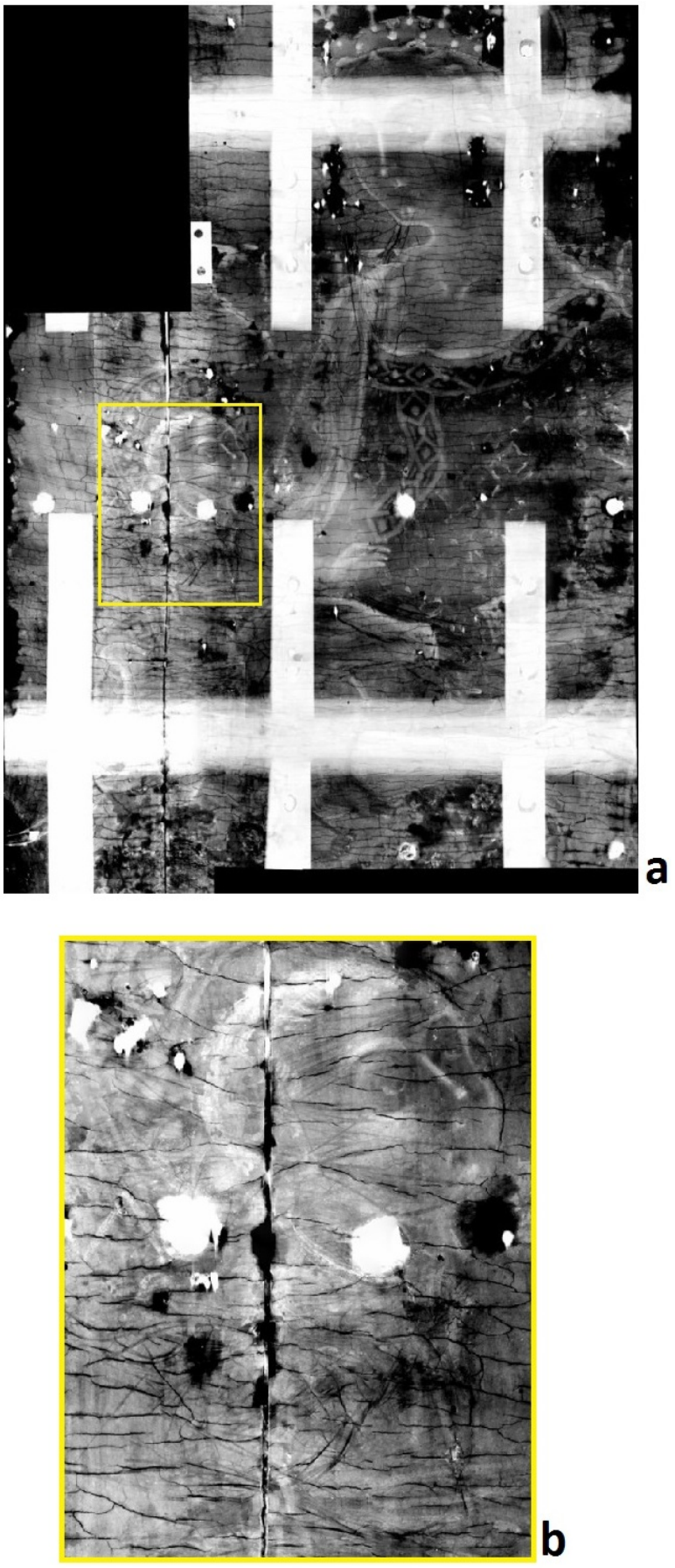

Figure A.2: a) RX of the Virgin and the Child, composed by 58 images, acquired with the Mo X-ray source at 29 kV, 19 mA, 0.18 mm Al filter and 2 s time of acquisition. b) Radiographic detail of the Child's face.

XVI century: The Trichiana Altarpiece

This large painting (Figure A.4) on canvas (238 x 176 cm) is attributed to Giovanni Da Mel (ca. 1480-1549), a renaissance Venetian artist dedicated to the *fresco* technique. Many frescoes have been attributed to him and his family in the valleys of the left side of the Piave river (near Belluno).
The peculiarity is that the altarpiece in the church of Trichiana (Prealps of Belluno) is the only painting on canvas attributed to him (1543).

As the displacement of the artwork to the Laboratory in Ferrara was precluded for its wide dimensions, the digital radiographies have been performed using a portable X-ray tube (EIS RX38: W anode) at the Restoration laboratory in Vittorio Veneto (TV)[1]. Some relevant details of the whole artwork have been acquired: the faces of the saints and the upper part of the Virgin Mary with the Child.

In the RX of the Virgin Mary (a in Figure A.5), as well as in the RX of the Saint (b), the details of the faces are not so evident, while the weft of the canvas is the most evident detail. This is due to a very thin pictorial layer. Furthermore, the sign of the compass to depict the halos does not continue under the faces, which means that halos are the last element sketched by the artist.

The XRF analysis performed *in situ* with the ARTAX200[2] and the microchemical analysis on some little samples characterized both the materials and the artistic techniques of this work of art. The results are reported in the following table (Figure A.3).

Colour/layer	Materials/pigments	XRF	SEM	Spot test
Preparation	Gypsum + Animal Glue	x	x	x
Imprimitura	White Lead	x	x	
White	White Lead	x	x	
Blue	Smalt	x	x	
Green	Copper Green	x	x	
	Green Earth	x		
Yellow	Lead–Tin Yellow	x		
	Yellow Ochre	x		
Brown	Brown Earth	x	x	
Red	Cinnabar	x	x	
	Red Earth	x	x	
	Red Lacquer		x	
	Minium	x	x	
Skin	White Lead + Cinnabar+ Red Earth	x	x	
Black	Organic Black (bones black) + Copper Green	x	x	
Technique	Oil			x

Figure A.3: Results of the XRF and microchemical analyses

[1]Restoration workshop Emanuela Ruggio, "la conservazione dell'arte", Vittorio Veneto (Italy)
[2]Bruker GmbH (Germany)

Figure A.4: Giovanni Da Mel, *Trichiana Altarpiece*, 1543, oil on canvas, 238 x 176 cm, Trichiana

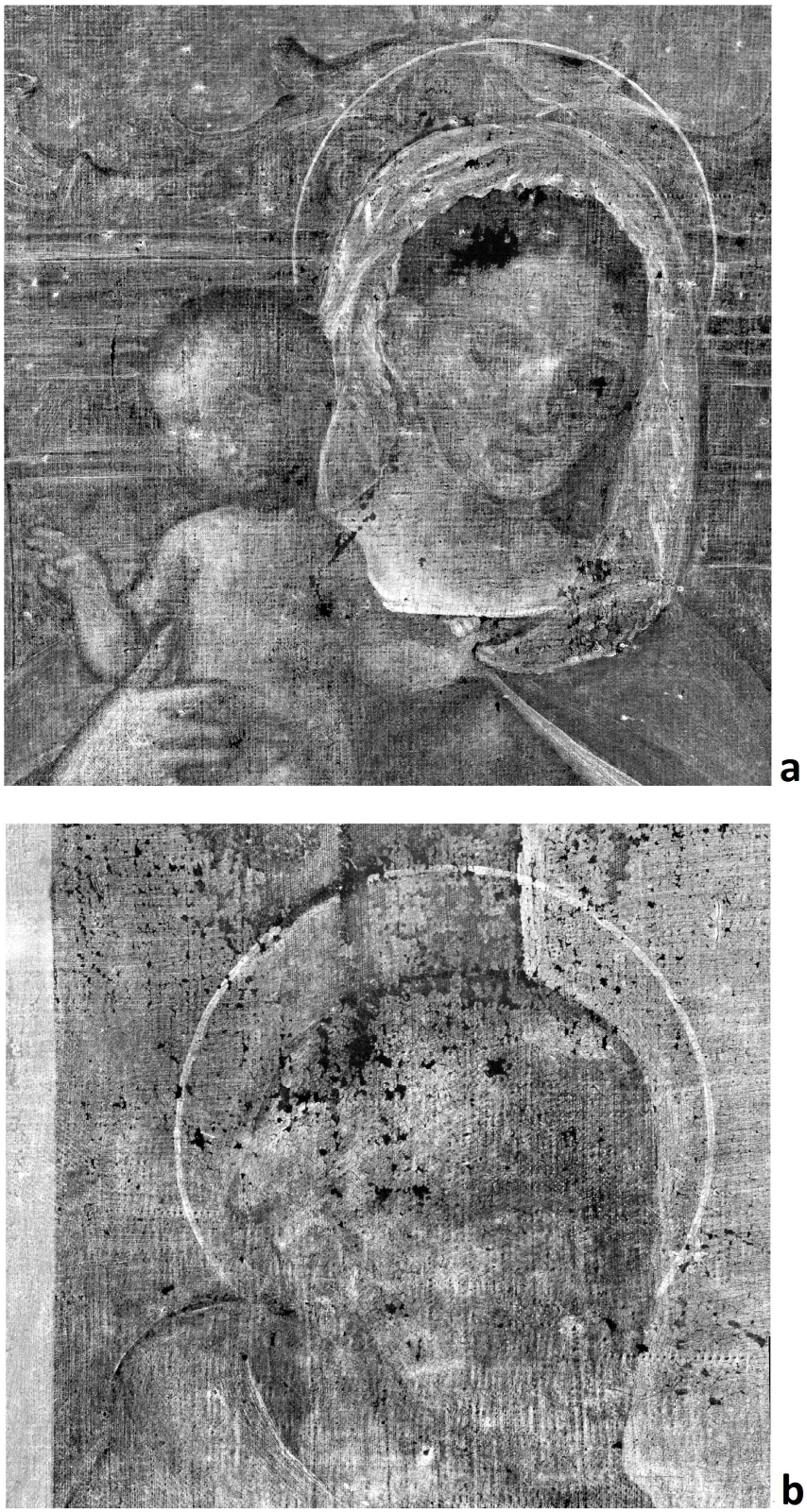

Figure A.5: Radiographies of the Trichiana Altarpiece. a) Virgin Mary and the Child, b) St. Bernardino. RX acquired at 25 kV, 0.5 mA and 6 s acquisition time.

Adoration of the Three Wise Men

This small wooden board, representing the Adoration of the Three Wise Man, is part of the Cretan Renaissance developed in Venice in the XVI century (Figure A.6).

Figure A.6: Cretan school, *Adoration of the Three Wise Men*, XVI century, Udine

The radiography has been acquired with the new scanner at the laboratories of the Dept. of Physics and Earth Science of the University of Ferrara. The aim was to identify the presence of retouches and restoration. From the Figure A.7, some restorative operations are visible, such as plastering (clearer) and little retouches (darker).

Figure A.7: Radiography of the Adoration composed by images. The Mo X-ray tube has been set at 25 kV, 19 mA, 0.2 mm Al filter, 1.5 s time of acquisition.

XVII century: Judith with the head of Holofernes

The painting of the XVII century (Figure A.8) is attributed to the workshop of Orazio Gentileschi. A strong doubt about the realization of the head of Judith exists. It seems the it could be painted by a second hand, not the one of the artist.

The radiography (Figure A.9) has been made to verify the retouch on the Judith face and has been acquired at the LARIX of the University of Ferrara. From the radiography, it is evident that the face of Judith has supported retouches and restorations, more evident in the left border of the face and on the neck, which appear darker than the closer areas (Figure A.10).

Figure A.8: Gentileschi workshop, *Judith and her maidservant with the head of Holofernes*, XVII century, oil on canvas, dim, private collection

Figure A.9: RX of Judith with the head of Holofernes composed by 266 images. The Mo X-ray tube has been set at 24 kV and 19 mA. The acquisitions lasted 1s.

Figure A.10: Detail of the Judith's face: a) color photo, b) radiography

XX century: Still Life

This XX century painting on canvas depicting a "Still Life" (Figure A.12), has been analysed with the old scanner at the LARIX Laboratory (University of Ferrara). The radiography and the XRF analysis have been performed before the restoration.

The preliminary observation of the painting have highlighted some details in disagreement with the subject represented. The radiography have clarified them, revealing an ancient painting underlying the Still life (Figure A.13). It illustrates the scene of Jacob's receiving the bloody tunic of Joseph. From the left, there is Rachel, the mother of Joseph, crying, then Jacob shocked and five Joseph's brothers.

The XRF analysis (Figure A.11) has been performed in order to discriminates the materials of the Still Life and of the underneath scene, trying to identify the period of execution. The pictorial materials are compatible with a painting of the XVII century, as the iconography of the artwork suggests.

	Still Life	Ancient painting
White	titanium white	lead white
Yellow	lead based yellow and zinc yellow	
Orange	minium/yellow pigments + earths or ochres	
Red	minium/english red	minium and cinnabar
Pink	titanium white/fast white, mixed with reds	
Skin		lead white + cinnabar + earths
Blue	azurite + Prussian blue + Paris blue + ultramarine blue	
Green	Cinnabar green, earths mixed with lead based yellow	
Brown	iron based pigments, organic pigments, + lead yellow pigment	burnt Sienna earth
Preparation		gypsum + animal glue + earths

Figure A.11: Material hypothesis from the XRF analysis

Figure A.12: Anonymous, *Still life*, XX century, oil on canvas, 129 x 101 cm, private collection

Figure A.13: Radiography of the Still Life. 170 radiographic images have been acquired with the W X-ray tube at 24 kV, 19 mA, 1 mm Al filtered, 1 s time of acquisition.

Hector and Andromache

In the production of Giorgio De Chirico (1888-1978), Hector and Andromache is one of the most famous theme painted by the metaphysics artist, who realized many versions of it. One is the painting of the 1958 conserved at the Remo Brindisi Museum (Lido di Spina) shown in Figure A.14.

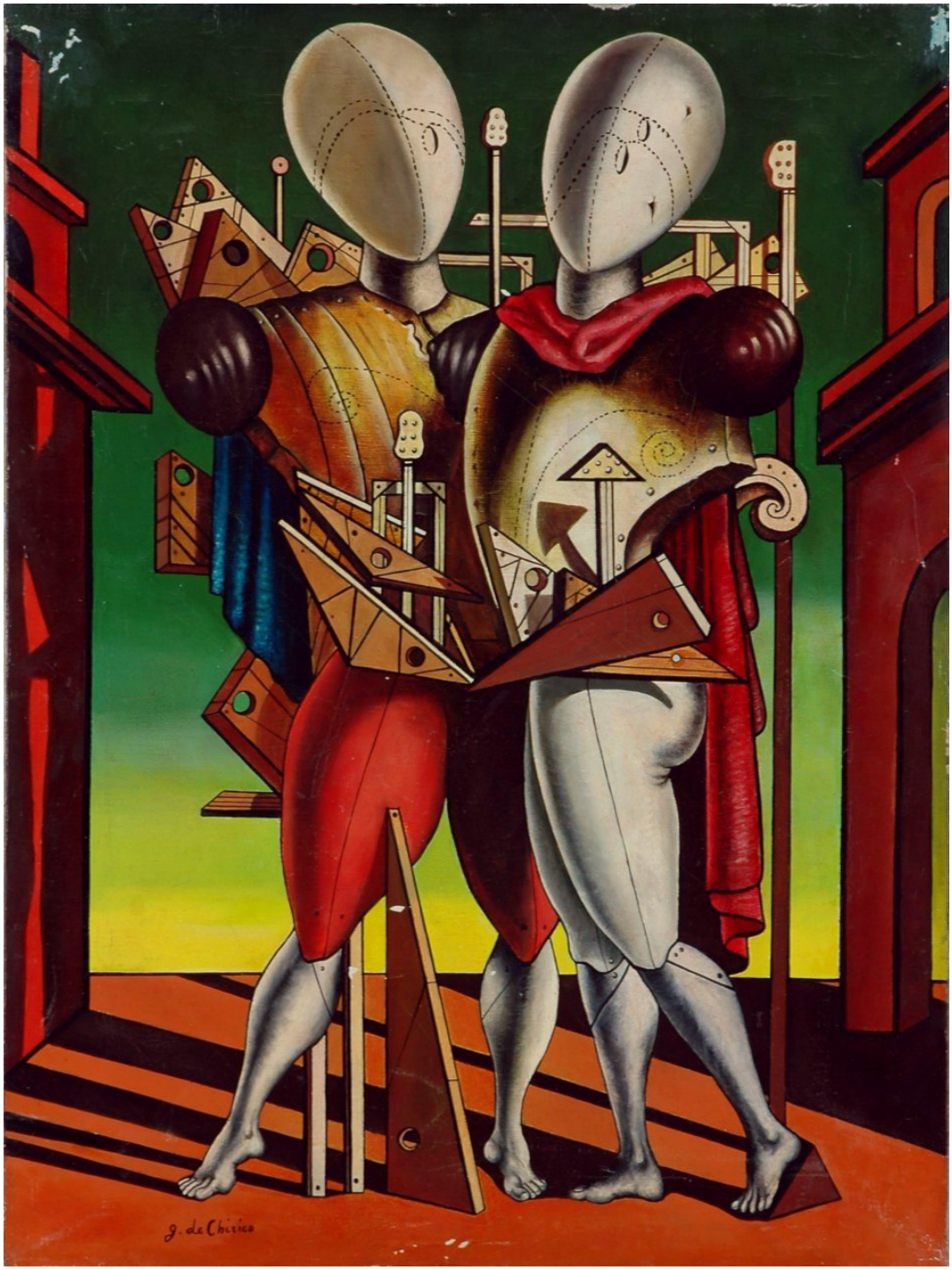

Figure A.14: Giorgio De Chirico, *Hector and Andromache*, 1958, acrylic on canvas, 80 x 60 cm, Remo Brindisi Museum, Lido di Spina

Thanks to the collaboration with the Museum, many imaging techniques have been applied to the paintings of the collection. In Figure A.15, the detail of the IR reflectography of this canvas shows the draft of the decoration of the armour.

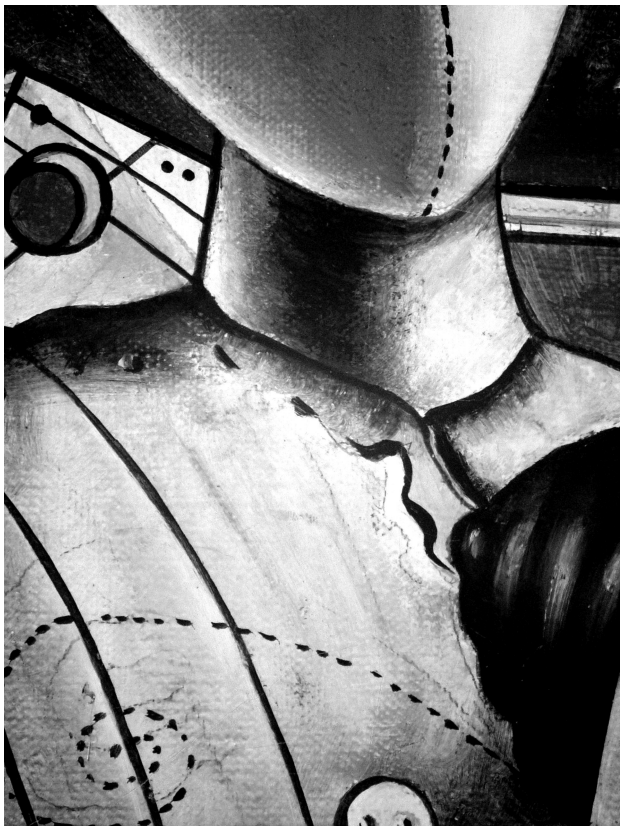

Figure A.15: IR detail of the Hector armour

Furthermore, even if the painting is modern and the pigments are mostly organic, the XRF analysis has permitted to make some hypothesis on them. They are reported in Figure A.16.

Colour	Pigments
Preparation	zinc white
White	Zn white, Ti white, Pb white
Yellow	Cr yellow, Ba yellow, Sr yellow
Orange	ochres, earths, Ba yellow, Sr yellow, Cr orange
Brown	ochres, earths, bone black
Red	ochres, earths, Cd red, Minium
Green	Cr green, Zn white, Fe and Cu based green
Blue	Fe and Cu based blue

Figure A.16: Table of the materials supposed by the XRF results

The radiography (Figure A.17) has been acquired at the LARIX at the University of Ferrara. The more evident element of the painting is the canvas, it is due to a very thin pictorial layer and to the use of organic pigments.

Figure A.17: Radiography of Hector and Andromache composed by 80 images. The W X-ray tube has been set at 20 kV, 19 mA, 0.5 mm of Al filter, 1.5 s time of acquisition.

Bibliography

[1] Impallaria A., Tisato F., Petrucci F., Dal Colle M., Ruggio E., *The palette of a XVI century Venetian artist: materials and methods of Giovanni Da Mel*, Books of Abstract of YOCOCU 2016, 5th international conference, 21-23 Sept. 2016, Madrid (Spain)

[2] Grassi N., Giuntini L., Mandò P.A., Massi M., *Advantages of scanning-mode ion beam analysis for the study of Cultural Heritage*, Nucl. Instr. and Meth. in Phys. Res. B 256 (2007) 712-718

[3] Re A., Angelici D., Lo Giudice A., Corsi J., Allegretti S., Biondi A. F., Gariani G., Calusi S., Gelli N., Giuntini L., Massi M., Taccetti F., La Torre L., Rigato V., Pratesi G., *Ion Beam Analysis of the provenance attribution of lapis lazuli used in glyptic art: The case of the "Collezione Medicea"*, Nucl. Instr. and Meth. in Phys. Res. B 348 (2015) 278-284

[4] Giuntini L., Massi M., Calusi S., Castelli L., Carraresi L., Fedi M.E., Gelli N., Liccioli L., Mandò P.A., Mazzinghi A., Palla L., Romano F.P., Ruberto C., Taccetti F., *Wide area scanning system and carbon microbeams at the external microbeam facility of the INFN LABEC laboratory in Florence*, Nucl. Instr. and Meth. in Phys. Res. B 348 (2015) 14-17

[5] Pichon L., Moignard B., Lemasson Q., Pacheco C., Walter P., *Development of a multi-detector and systematic imaging system on the AGLAE external beam*, Nucl. Instr. and Meth. in Phys. Res. B 318 (2014) 27-31

[6] Albéric M., Müller K., Pichon L., Lemasson Q., Moignard B., Pacheco C., Fontan E., Reiche I., *Non-invasive quantitative micro-PIXE-RBS/EBS/EBS imaging reveals the lost polychromy and gilding of the Neo-Assyrian ivories from the Louvre collection*, Talanta 137 (2015) 100-108

[7] Ruberto C., Mazzinghi A., Massi M., Castelli L., Czelusniak C., Palla L., Gelli N., Betuzzi M., Impallaria A., Brancaccio R., Peccenini E., Raffaelli M., *Imaging study of Raffaello's "La Muta" by a portable XRF spectrometer*, Microchemical Journal 126 (2016) 63-69

[8] Alfeld M., Janssens K., Dik J., de Nolf W., van der Snickt G., *Optimization of mobile scanning macro-XRF system for the in situ investigation of historical paintings*, J. Anal. At. Spectrom. 26 (2011) 899-909

[9] Van der Snickt G., Legrand S., Caen J., Vanmeert F., Alfeld M., Janssens K., *Chemical imaging of stained-glass windows by means of macro X-ray fluorescence (MA-XRF) scanning*, Microchemical Journal 124 (2016) 615-622

[10] Ricciardi P., Legrand S., Bertolotti G., Janssens K., *Macro X-ray fluoscence (MA-XRF) scanning of illuminated manuscript fragments: potentialities and challenges*, Microchemical Journal 124 (2016) 785-791

[11] Santos H. C., Caliri C., Pappalardo L., Catalano R., Orlando A., Rizzo F:, Romano F. P., *Identification of forgeries in historical enamels by combining the non-destructive scanning XRF imaging and alpha-PIXE portable techniques*, Microchemical Journal 124 (2016) 241-246

[12] *https://www.bruker.com/products/x-ray-diffraction-and-elemental-analysis/micro-xrf-and-txrf/m6-jetstream/overview.html* (last consultation 7 Nov 2016)

[13] Romano F.P., Caliri C., Cosentino L., Gammino S., Giuntini L., Mascali D., Neri L., Pappalardo L., Rizzo F., Taccetti F., *Macro and Micro Full Field X-ray Fluorescence with an X-ray pinhole camera presenting high energy and high spatial resolution*, Anal. Chem. 86 (2014) 10892-10899

[14] Lehmann L. A., Alvarez R. E., Macovski A., Brody W. R., Pelc N. J., Riederer S. J., Hall A. L., *Generalized image combinations in dual KVP digital radiography*, Medical Physics 8 (1981) 659-667

[15] *https://www.nist.gov/pml/x-ray-form-factor-attenuation-and-scattering-tables*

[16] Sarnelli A., Taibi A., Tuffanelli A.,Baldazzi G., Bollini D., Cabal Rodriguez A. E., Gombia M., Prino F., Ramello L., Tomassi E., Gambaccini M., *K-edge digital subtraction imaging based on a dichromatic and compact x-ray source*, Phys. Med. Biol. 49 (2004) 3291-3305

[17] Baldelli P., Taibi A., Tuffanelli A., Gilardoni M. C., *A prototype of a quasi-monochromatic system for mammography applications*, Phys. Med. Biol. 50 (2005) 2225-2240

[18] Krug K., Dik J., Den Leeeuw M., Whitson A., Tortora J., Coan P., Nemoz C., Bravin A., *Visualisation of pigment distributions in paintings using synchroton K-edge imaging*, Appl. Phys A 83 (2006) 247-251

[19] Albertin F., Franconieri A., Gambaccini M., Moro D., Petrucci F., Chiozzi S., *A quasi-mochromatic X-ray source for art painting pigments investigation*, Appl. Phys. A 96 (2009) 503-510

[20] Kikpatrick P., *On the theory and use of Ross filters*, Review of Scientific Instruments 10 (1939) 186

[21] Kikpatrick P., *On the theory and use of Ross filters. II*, Review of Scientific Instruments 15 (1944) 223

[22] Cardarelli P., Di Domenico G., Marziani M., Mucollari I., Pupillo G., Sisini F., Taibi A., Gambaccini M., *Energy distribution measurement of narrow-band ultrashort x-ray beams via K-edge filters subtraction*, J. Appl. Phys. 112 (2012) 074908

[23] Re A., Albertin F., Bortolin C., Brancaccio R., Buscaglia P., Corsi J., Cotto G., Dughera G., Durisi E., Ferrarese W., Gambaccini M., Giovagnoli A., Grassi N., Lo Giudice A., Mereu P., Mila G., Nervo M., Pastrone N., Petrucci F., Prino F., Ramello L., Ravera M., Ricci C., Romero A., Sacchi R., Staiano A., Visca L., Zamprotta L., *Results of the Italian neu_ART project*, IOP Conf. Ser.: Materials Science and Engineering 37 (2012) 012007

[24] Mucollari I., *K-edge filter subtraction technique used for mapping elemental distribution on paintings*, PhD thesis, years 2011/2013

[25] Albertin F., Gambaccini M., Petrucci F., Gargano M., Ludwig N., Milazzo M., Pedrielli F., Chiozzi S., Evangelisti F., *Nuove applicazioni della radiografia digitale alla diagnostica dei dipinti*, Proc.of Elettroottica 2008, B.3-38. AEIT, Milan (2008)

[26] Albertin F., Boselli L., Chiozzi S., Peccenini E., Pellicori V., Petrucci F., Poldi G., Tisato F., *La radiografia e le diagnostiche fisiche del dipinto Madonna con Bambino tra san Rocco e san Sebastiano di Giovanni da Mel*, Progetto Restauro, 65, 40-48 (2013)

[27] Impallaria A., Evangelisti F., Petrucci F., Tisato F., Castelli L., Taccetti F., *A new scanner for in situ digital radiography of paintings*, Appl. Phys. A 122 (2016) 1043

[28] Albertin F., *K-edge radiography and applications to Cultural Heritage*, PhD thesis, year 2011